MOESSBAUER SPECTROSCOPIC AND RELATED CHARACTERIZATION OF FISCHER-TROPSCH CATALYSTS

PENNSYLVANIA STATE UNIV., UNIVERSITY PARK. DEPT. OF MATERIALS SCIENCE AND ENGINEERING

MAR 1981

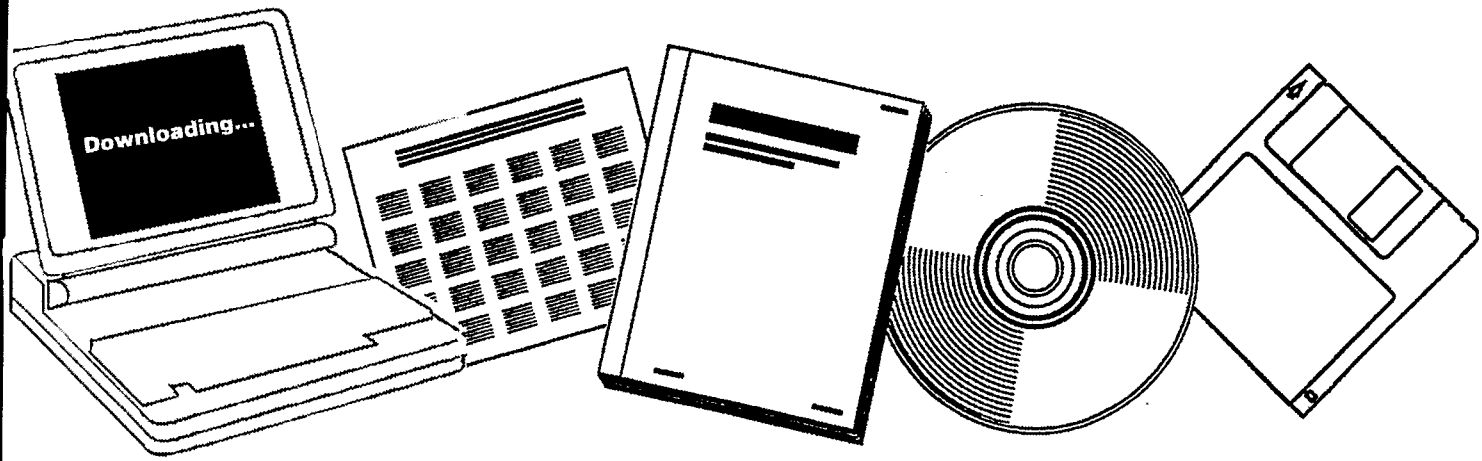

One Source. One Search. One Solution.

NTIS

Providing Permanent, Easy Access to U.S. Government Information

National Technical Information Service is the nation's largest repository and disseminator of government-initiated scientific, technical, engineering, and related business information. The NTIS collection includes almost 3,000,000 information products in a variety of formats: electronic download, online access, CD-ROM, magnetic tape, diskette, multimedia, microfiche and paper.

Search the NTIS Database from 1990 forward

NTIS has upgraded its bibliographic database system and has made all entries since 1990 searchable on **www.ntis.gov.** You now have access to information on more than 600,000 government research information products from this web site.

Link to Full Text Documents at Government Web Sites

Because many Government agencies have their most recent reports available on their own web site, we have added links directly to these reports. When available, you will see a link on the right side of the bibliographic screen.

Download Publications (1997 - Present)

NTIS can now provides the full text of reports as downloadable PDF files. This means that when an agency stops maintaining a report on the web, NTIS will offer a downloadable version. There is a nominal fee for each download for most publications.

For more information visit our website:

www.ntis.gov

U.S. DEPARTMENT OF COMMERCE
Technology Administration
National Technical Information Service
Springfield, VA 22161

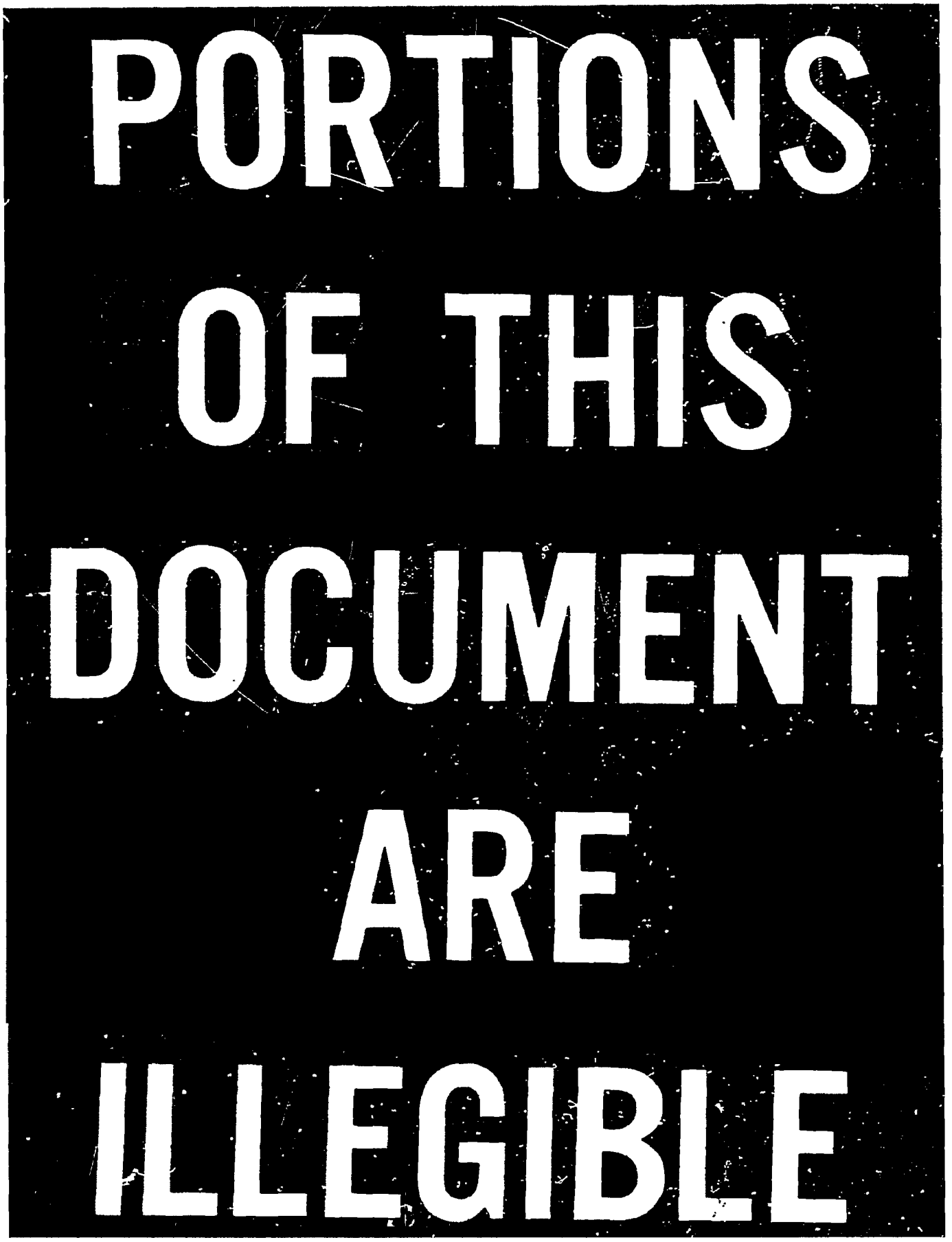

ANNUAL REPORT

Contract No. DE-AC-22-79PC10350

Mössbauer Spectroscopic and Related Characterization of Fischer-Tropsch Catalysts

submitted by

Prof. L. N. Mulay
Materials Science and Eng. Dept.
136 Materials Research Lab.
PENNSYLVANIA STATE UNIVERSITY
UNIVERSITY PARK
(STATE COLLEGE), PA. 16802

to

UNITED STATES DEPARTMENT OF ENERGY
PITTSBURGH ENERGY TECHNOLOGY CENTER
P.O. BOX 10940
PITTSBURGH, PENNSYLVANIA 15236

March 1981

DOE/PC/10350--T1

Mössbauer Spectroscopic and Related Characterization of Fischer-Tropsch Caralysts

Contract No. DE-AC-22-79PC1035

Forward

This annual report for the year ending February 28, 1981, is based on the M.S. thesis in Applied Physics recently submitted by Mr. Cary C. Lo. The work was done under the direction of Dr. L.N. Mulay, Professor of Solid State Science at The Pennsylvania State University, University Park, PA 16802.

The report gives details of (i) the expensive instrumentation (most of which was not purchased from DOE type federal funds,) (ii) the planning of experiments, (iii) the necessary sophisticated theoretical background for the experiments performed, and finally, (iv) a careful interpretation of the results for which new theoretical and computational expertise had to be developed.

Mr. Lo was given a half-time graduate assistantship for about 3 terms. The Physics Department provided him with a teaching assistantship to help him and the principal investigator to complete the research and development work for the above DOE Contract. Dr. K.R.P.M. Rao worked as a part-time research associate on the project to set up our new instrumentation and returned to India in mid-October 1980.

The research will appear in the form of a chapter in "Recent Chemical Applications of Mössbauer Spectroscopy" in July 1981 (American Chemical Society Monograph Series) and will result in several other publications. These publications will be co-authored by research collaborators from PETC. The principal investigator wishes to acknowledge the enthusiastic cooperation received from Drs. Blaustein, Rao and Schehl.

April 1981

L.N. Mulay
Professor of Solid State Science
The Pennsylvania State University
University Park, PA 16802

Abridged Table of Contents

ABSTRACT

Medium pore (dia ~6Å) zeolites such as ZSM-5 and Silicalite impregnated with Group VIII metals provide selective catalytic pathways for the conversion of coal-derived synthesis gas to gasoline or olefins. Mössbauer and magnetic studies on these catalysts containing Fe or Fe + Co are reported. The zeolites were impregnated with metal nitrate solutions, reduced and carbided to yield the active catalyst. The freshly impregnated samples showed Fe^{3+} type spectra. The ZSM-5 (14.7% Fe) and Silicalite (13.6% Fe) samples exposed to H_2 (450°C) showed ~85% reduction to the metallic state. The carbided ZSM-5 (14.7% Fe) revealed a spectrum of Hagg carbide (Fe_5C_2), an active component of the catalyst. The used catalysts showed mixtures of Hagg carbide (Fe_5C_2) and cementite (Fe_3C). It is suggested that the selectivity of ZSM-5 (5.6% Fe, 4.5% Co) resulted from Fe-Co alloy formation.

TABLE OF CONTENTS

Table of Contents (Cont.)

LIST OF TABLES

(I) The background information and the research objectives have been presented above;

(II) Theoretical aspects of Mössbauer spectroscopy and magnetic measurements;

(III) Experimental techniques;

(IV) Discussion of results obtained.

LIST OF FIGURES

List of Figures (Cont.)

ACKNOWLEDGEMENTS

I would like to gratefully acknowledge Professor Mulay for his guidance throughout this research project and his critical editing of the thesis. I would like to thank the Department of Energy for awarding a Contract No. DE-AC-22-79 PC 1035 to Professor Mulay for supporting the research reported here, and for providing partial financial assistance to me. I would also like to thank Professors R. H. Good, Jr. and E. Bleuler, Department of Physics, for providing occasional teaching assistantships. Dr. K. R. P. M. Rao (of the Bhabha Atomic Research Center, Bombay, India), who spent a year (1979-80) in Professor Mulay's laboratory, helped in setting up the new Austin Mössbauer Spectrometer. I wish to acknowledge Dr. V. U. S. Rao (of the Pittsburgh Energy Technology Center, Pittsburgh, PA) for his overall assistance with the catalysis studies on the samples reported in this thesis. I thank Professor G. R. Barsch for serving on my committee and for a critical reading of the manuscript.

My thanks are also extended to my friends and colleagues, Dr. F. C. Twu, Mr. A. V. Prasada Rao, and Mr. M. Oskooie-Tabrizi, for their valuable suggestions during the course of the experimental work.

I. INTRODUCTION

A. General Background

During the past few decades, the Fischer-Tropsch process has been used for CO/H_2 synthesis gas conversion to obtain the production of a large fraction of gasoline range hydrocarbons, etc. (1,2). The Fischer-Tropsch process is several years old. It was started since Sabatier's work in 1902 and further developed by Fischer and Tropsch during the 1920-1935 period in Germany. It was used extensively in Germany during World War II to produce aviation and other fuels. Among the first few Fischer-Tropsch plants one has been in operation (known as Sasol I) since 1955, in Sasolburg, South Africa. The increasing annual rate of oil price has renewed the interest of researchers in the production of fuels and chemicals, such as C_4-C_{10} paraffins, olefins, propylene, or ethylene, from CO/H_2 synthesis reactions. The recent Mobil Oil Company patents also use F-T process for alcohols and hydrocarbons. Although the technology has advanced through mostly empirical approaches, very little is known about the precise role and reaction mechanism of F-T synthesis such as sulfur poisoning, carbon deposition, product selectivity, and thermal degradation (3). Although catalysis is not a phenomenon awaiting a unique explanation, it is still elusive in many ways. For instance, the questions concerning the structure and electronic property correlations of the catalysts on the one hand, and the correlations of the electronic properties of catalysts with their activity, on the other hand, have not yet been fully explored. With supported metal catalysts, the questions concerning any metal support interations and their role, if any, and the nature of the catalysis are still open to question.

The Fischer-Tropsch process was started by Sabatier and Senderens in 1902, developed by Fischer and Tropsch in 1935, and further improved by Pichler in 1938. Hundreds of references have been published in this area during the past eighty years, but a detailed review is beyond the scope of this thesis. However, several books and reviews (4-8) which have appeared recently in the catalysis literature are presented.

B. Research Objectives

A review of the literature on the synfuel conversion using F-T catalysts showed a need for seeking answers to the following situations.

(i) To see if an overall increase in catalytic activity can be brought about by introducing a fine dispersion of Fe or Fe-Co bimetallic clusters in unusual zeolite-type cage structures.

(ii) To identify the nature of the species formed in the preparation of the fresh, reduced, carbided and used catalysts.

(iii) To seek correlations between the species formed, their electronic properties and the actual synfuel conversion process.

C. Outline of the Thesis

In an effort to seek answers to the type of situations discussed before, it was decided to study the Fe^{57} Mössbauer spectra and magnetic properties of the fresh, reduced, carbided and used catalysts. These techniques indeed provide a sensitive probe for seeking information at the microscopic and macroscopic level.

The work carried out is presented in this thesis in the following chapters.

II. THEORETICAL ASPECTS

A. Mössbauer Spectroscopy

1. History

The Mössbauer effect was discovered by R. L. Mössbauer (9) in 1958. Because of this discovery he won the Nobel prize in 1961. This extremely high resolution technique was then quickly expanded from nuclear and solid state physics to chemistry, biology and metallurgy. A number of good books (10-15) discuss in detail Mössbauer spectroscopy with regard to its theory and applications. Recently a series of reviews (16-20) on the Mössbauer spectroscopy have been presented in the application of catalysis. In addition there are annual compilations of all references on Mossbauer spectroscopy, published by Wiley-Interscience, New York.

In principle, the valence state and bonding type of an atom in the solid, the symmetry of the electric field surrounding an atom, the presence and magnitude of a magnetic field and electronic structure of an atom all can be determined from Mössbauer measurements. But the limited number of isotopes suitable for the effect does not make Mössbauer spectroscopy applicaable to all materials. However, the most valuable iron catalysts can be studied (21-33) by using Mössbauer technique, because of the relatively good abundance of Fe^{57} in such materials and because Fe^{57} provides a transition in low range energy spectrum (14.4 KeV).

The essential feature of Mössbauer effect is due to nuclear resonance absorption of γ-rays. Suppose a nucleus in an excited state of energy E_e comes back to the ground state of energy E_g by emitting

a gamma ray of energy $E_o = E_e - E_g$. This quantum energy E_o may be totally absorbed by another nucleus with the same number of protons Z and same number of neutrons N in its ground state. Therefore transition to the excited state of energy E_e takes place. This phenomenon is called nuclear resonance absorption of γ-rays (see Figure 1). Before the discovery of the Mössbauer effect it could not be observed because of the recoil effect.

It is known from nuclear physics that if a γ-ray is emitted from an excited nucleus of mass M with energy $E_o = E_e - E_g$, it experiences a recoil. A recoil energy E_R due to the nucleus moving with a velocity $\vec{v}$ in opposite direction to that of the γ-ray emission takes place (see Fig. 2).

$$E_R = (1/2)Mv^2 \tag{1}$$

The momentum of the emitted gamma ray is given by

$$P_\gamma = E_\gamma/c \tag{2}$$

where $E_\gamma = E_o - E_R$ is the energy of the emitted γ-ray, c is the velocity of light.

From conservation of momentum

$$P_n = -P_\gamma = -E_\gamma/c \tag{3}$$

where P_n is the momentum of the nucleus and,

$$E_R = P_n^2/2M = P_\gamma^2/2M = E_\gamma^2/2Mc^2 \tag{4}$$

Because of the large mass of the nucleus, E_R is very small compared to E_o such that we may assume

$$E_\gamma = E_o - E_R \tilde{\sim} E_o \quad .$$

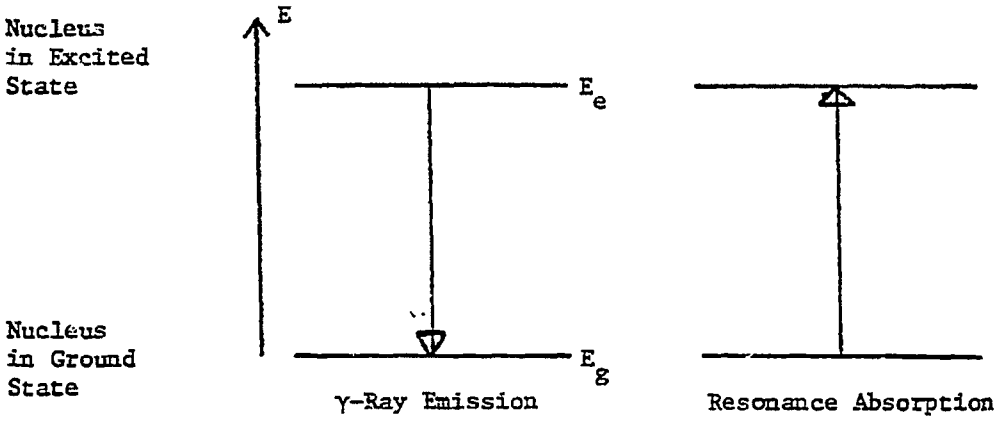

Figure 1. Nuclear resonance absorption of γ-ray

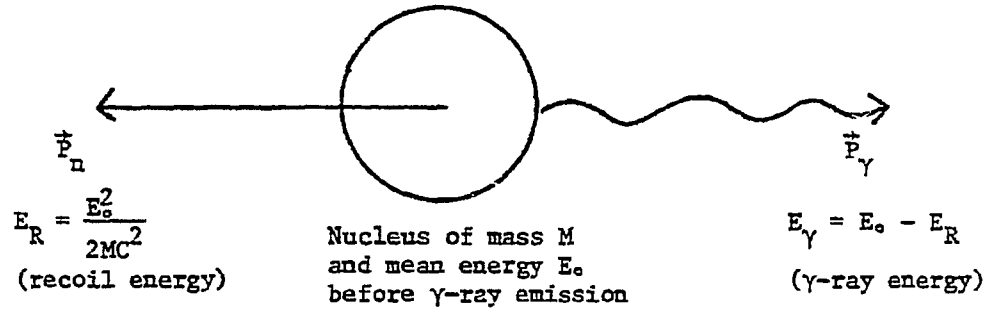

Figure 2. Recoil of momentum $\vec{P}_n$ and energy E_R imparted to an isolated nucleus upon γ-ray emission

From Eq. 4,

$$E_R = E_o^2/2Mc^2 \tag{5}$$

In the case of ^{57}Fe, the transition between the first excited state and the ground state $E_o = 14.4$ keV (see Figure 3). The recoil energy of a ^{57}Fe nucleus is

$$E_R = \frac{(14.4 \text{ keV})^2}{2 \times (56.95 \text{ amu})(931 \text{ MeV/amu})}$$

$$= 1.95 \times 10^{-3} \text{ eV}$$

This means the recoil effect reduces the emitted γ-ray from E_o to a smaller energy by E_R (see Figure 4). In other words, the γ-ray requires the total energy $E_\gamma = E_o + E_R$ to make up the recoil effect. If the natural line width Γ is smaller than E_R, there will be no absorption of γ-rays since no overlap occurs between transitions.

From the Heisenberg uncertainty relation it is known that the energy of each emitted gamma ray is not exactly the same (see Figure 5).

$$\Delta E \, \Delta t \geq \frac{h}{2\pi} \tag{6}$$

where Δt = uncertainty in time

h = Plank's constant

Nuclear transitions take place in all possible energies within the range of ΔE. The uncertainty in the energy of the emitted gamma ray ΔE is just the line width Γ when the uncertainty in the time of emission Δt is in the order of the mean lifetime τ. Therefore,

$$\Gamma\tau = \frac{h}{2\pi} \tag{7}$$

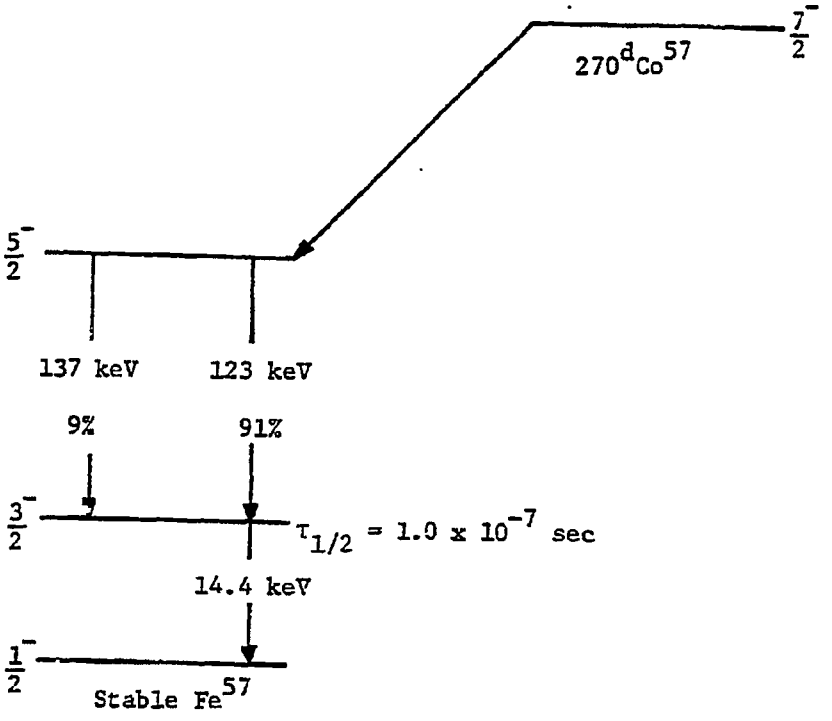

Figure 3. The decay of ^{57}Co to stable ^{57} Fe

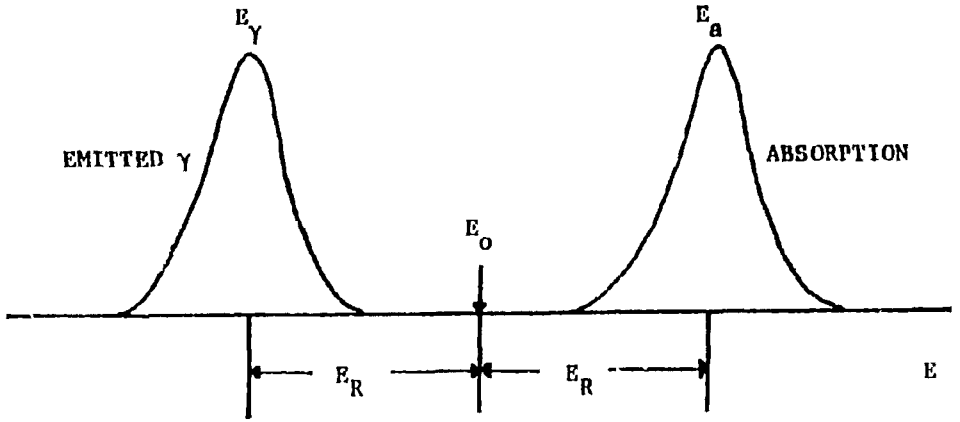

Figure 4. Resonant absorption is not possible since there is no overlap between emission and absorption line.

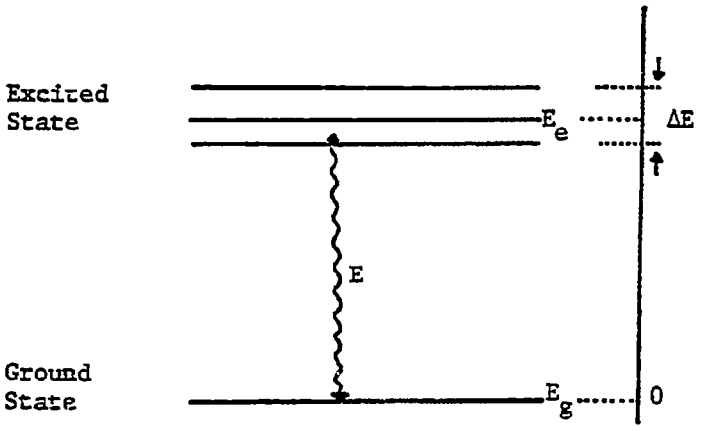

Figure 5. $\Delta E = \Gamma = h/\tau$ is the energy width of the excited state with a mean lifetime τ due to Heisenberg uncertainty relation.

where Γ = the full width of the transition line at half maximum

τ = mean lifetime of the excited state

For ^{57}Fe the natural line width is

$$\Gamma = \frac{\ln^2 \hbar}{\tau_{1/2}} = \frac{0.63(6.582 \times 10^{-16} \text{ eV-sec})}{97.81 \times 10^{-9} \text{ sec}} = 4.66 \times 10^{-9} \text{ eV} \tag{7a}$$

This is about six orders of magnitude smaller than the recoil energy of a ^{57}Fe nucleus ($E_R = 1.95 \times 10^{-3}$ eV); hence, nuclear resonance absorption is not possible in isolated atoms.

Mössbauer found that the atom was more or less rigidly bound to the lattice in the solid state so that the recoil energy was distributed throughout the crystal. Therefore, the Eq. 4 for the recoil energy can be written as

$$E_R = \frac{E_\gamma^2}{2M_c c^2} \tag{8}$$

where M_c = mass of entire crystal.

Because of the very large mass of the crystallite as compared to the mass of a single nucleus, the recoil momentum is thus taken up by the whole crystal with practically no loss to the emitted gamma ray. Therefore, the gamma ray is able to be absorbed by another nucleus of the same kind. Mössbauer brought the emission and absorption lines into coincidence by using the Doppler effect.

The Mössbauer source line width affects the velocity resolution of its experiments (34). The experimentally observed spectral line

width (Γ exp) is a convolution of the source (Γ_s) and absorber (Γ_A) line widths. Theory predicts a Lorentzian shape of Mössbauer spectral line (Γ_M) equivalent to $\Gamma_s + \Gamma_A$. For source and absorber nuclei at infinite dilution in ideal environments $\Gamma_A = \Gamma_s = \Gamma$ (the nature line width), that is $\Gamma_M = 2\Gamma$. In the case of ^{57}Fe, from Eq. 7a

$$\begin{aligned}\Gamma &= 4.66 \times 10^{-9} \text{ eV} \times 1.6 \times 10^{-19} \text{ c/e} \\ &= 7.456 \times 10^{-28} \text{ J} \times 10^{7} \text{ erg/J} \\ &= 7.456 \times 10^{-21} \text{ erg} \times (6.625 \times 10^{-27} \text{ erg Mcs})^{-1} \\ &= 1.13 \text{ Mcs}^{-1} \times (11.61 \text{ Mcs}^{-1} \text{ mm}^{-1} \text{ s})^{-1} \\ &= 0.0969 \text{ mm/s} \end{aligned} \tag{9}$$

This is based on the assumption that the equilibrium positions of the velocity of the vibrating nuclei of the emitter and absorber are constant in time. In practice, deviations cause line-broadening such as diffusional motion of the atoms (lattice imperfections), temperature, etc., so that $\Gamma_A \neq \Gamma_s \neq \Gamma$. Γ_M is further modified by finite source and absorber thickness as reported (35-39). In measurements, Γ_M is written as

$$\Gamma_M = \Gamma_s + \Gamma_A + f(T_A) \tag{10}$$

where $f(T_A)$ is a function describing broadening due to finite absorber thickness T_A. By calculating the slope of a plot of Γ_M against absorber thickness (T_A), using Eq. 10 with $f(T_A) = 0.27\ \Gamma\ T_A$ (36); that spectral line width can be written as

$$\Gamma_M = \Gamma_s + \Gamma_A + 0.27\ \Gamma\ T_A \tag{11}$$

In the following sections various Mössbauer parameters are discussed.

2. Isomer Shift

The isomer shift (δ) arises due to the electrostatic interaction between the nuclear charge distribution and those electrons which have a finite probability of being found in the region of the nucleus. In general, this shift will be different in source and absorber, and is given by the following equation:

$$\delta = \frac{2\pi}{5} Ze^2(R_e^2 - R_g^2)(|\Psi_s(0)|^2_{ABS} - |\Psi_s(0)|^2_{SOURCE}) \qquad (12)$$

This equation shows that the isomer shift is proportional to the difference of the square of the radius of the excited and ground state nuclear radii (the nuclear term), and also to the difference in electron density between the source and absorber (the chemical term).

A difference in electron charge density can arise from differences in chemical environment. Even though s-electrons are the only electrons that have a finite probability of being found in the nucleus, p-, d-, and f-electrons also contribute a screening effect. For example, in the case of Fe^{2+} (di-valent) and Fe^{3+} (tri-valent), the screening for Fe^{2+} ($3d^6$) is greater than for Fe^{3+} ($3d^5$). Therefore, Fe^{2+} has lower 3s-electron density. This results in a higher isomer shift value for Fe^{2+} than for Fe^{3+} (remembering that $R_e^2-R_g^2$ is negative for ^{57}Fe). This isomer shift difference in $3d^5$ and $3d^6$ configurations in iron may be used to predict oxidation state in various compounds.

3. Quadrupole Interaction

The quadrupole interaction (e^2qQ) consists of the nuclear constant eQ for the resonant isotope and eq, which is a measure of the chemical environment such as charge deformations by the surrounding ligands and/or defects.

The isomer shift. (Eq. 12) was derived assuming the nucleus to be spherical and to have a uniform charge density. If there is a departure from spherical symmetry of the electric charge distribution then there will be a quadrupole splitting. This will depend on the magnitude of the quadrupole moment of the nucleus ($I > 1/2$), the electric field gradient (EFG) at the nucleus, and the electrostatic field generated from the valence electrons. For ^{57}Fe, $I_e = \frac{3}{2}$ and $I_g = \frac{1}{2}$, and the $I_e = \frac{3}{2}$ does split into two ($M_I = \pm \frac{3}{2}, \pm \frac{1}{2}$) while the $I_g = \frac{1}{2}$ remains degenerate since it has no quadrupole moment (see Figure 6). In such a case, a two-line spectrum is obtained and the separation of the peaks is the quadrupole splitting.

The electric field at the Mössbauer nucleus is the negative gradient of the potential, V:

$$E = -\nabla V \tag{13}$$

The EFG is the gradient of the electric field.

$$EFG = \nabla E = - \begin{vmatrix} V_{xx} & V_{xy} & V_{xz} \\ V_{yx} & V_{yy} & V_{yz} \\ V_{zx} & V_{zy} & V_{zz} \end{vmatrix} \tag{14}$$

where $V_{xx} = \frac{\partial^2 V}{\partial x^2}$, $V_{yx} = \frac{\partial^2 V}{\partial y \partial x}$, $V_{zx} = \frac{\partial^2 V}{\partial z \partial x}$, etc.

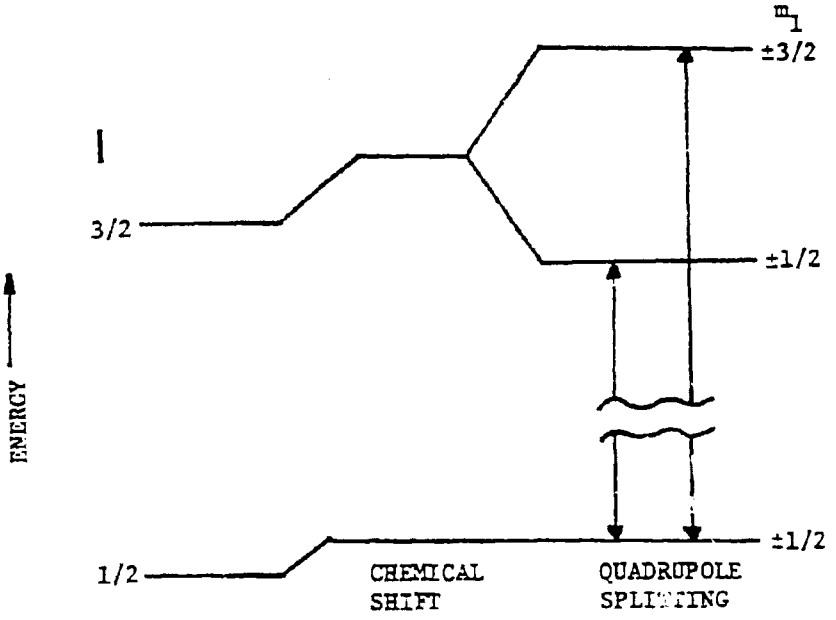

$$\Delta E_Q = 1/2e^2qQ(1 + \eta^2/3)$$

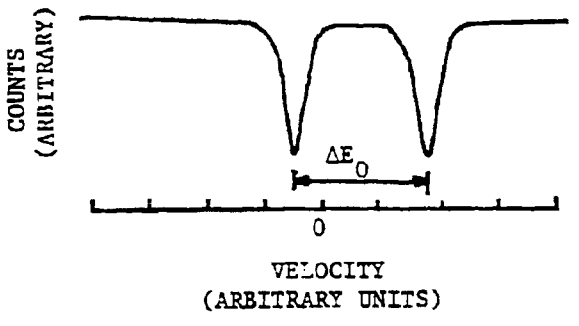

Figure 6. Energy levels and resulting spectrum of quadrupole splitting for ^{57}Fe

Normally the EFG axes are chosen in a diagonal form such that the EFG tensor has three non-zero components taken as $|V_{zz}| > |V_{yy}| \geq |V_{xx}|$. These three components can be reduced to two independent parameters V_{zz} and asymmetry parameter η, given by

$$\eta = \frac{V_{xx} - V_{yy}}{V_{zz}} \tag{15}$$

where $0 \leq \eta \leq 1$.

For ^{57}Fe the quadrupole splitting is given as

$$\Delta E_Q = 1/2e^2qQ^2(1 + \eta^2/3) \tag{16}$$

where Q is the nuclear quadrupole moment. The asymmetry parameter (η) vanishes in the case of high symmetry.

4. Hyperfine Interactions

Hyperfine interaction will occur if there is a magnetic field (H) at the nucleus either from magnetic ordering in the solid itself or from an externally applied magnetic field. The Hamiltonian describing the magnetic dipole hyperfine interaction is given by

$$H = -\hat{\mu}\cdot\hat{H} = -g\mu_N\hat{I}\cdot\hat{H} \tag{17}$$

where μ_N is the nuclear Bohr magneton ($e\hbar/2Mc$), $\hat{\mu}$ is the nuclear magnetic moment, $\hat{I}$ is the nuclear spin, and g is the nuclear g-factor ($g = \mu/I\mu_N$). The degeneracy of the energy levels of the nuclear magnetic dipole will be lifted by an amount of $(2I + 1)$, the energy of each level is given by

$$E_m = \frac{-\mu H m_I}{I} = -g\mu_N H m_I \tag{18}$$

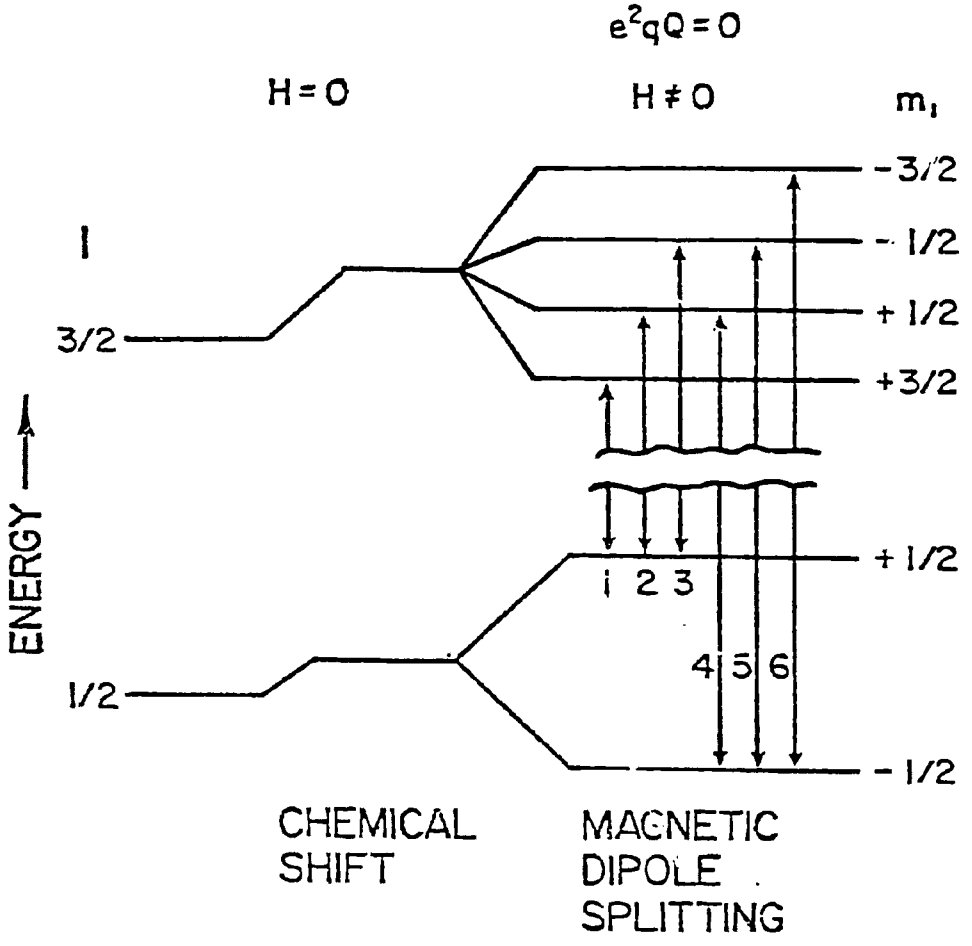

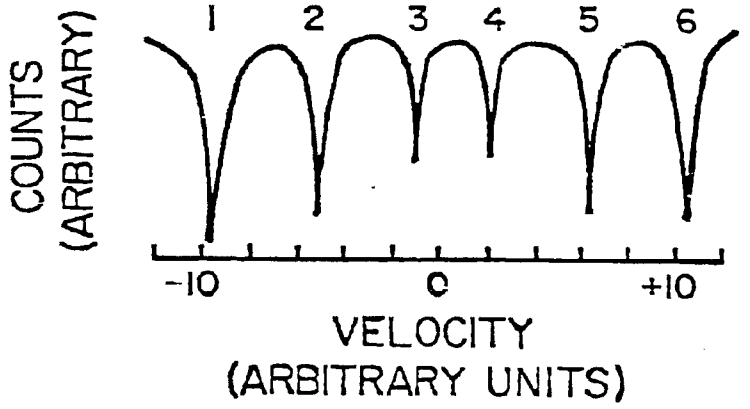

Figure 7. Energy levels and resulting spectrum of hyperfine magnetic interactions for ^{57}Fe.

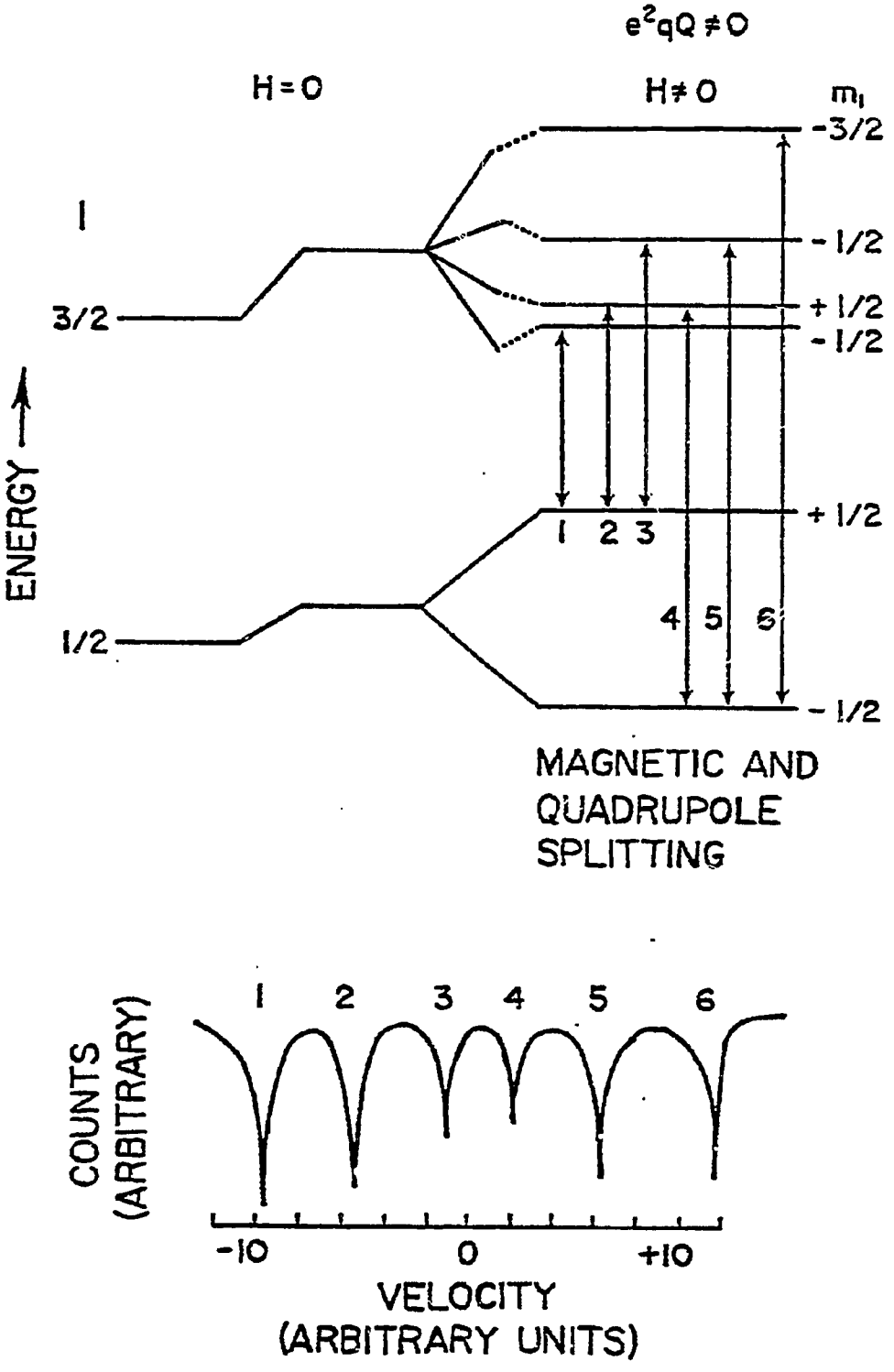

Figure 8. Combined magnetic and quadrupole interaction along with resulting spectrum.

where m_I is the nuclear magnetic quantum number. Six transitions which obey the selection rule ($\Delta m_I = \pm 1, 0$) produce a six-line spectrum, as shown in Figure 7.

5. Combined Magnetic and Electric Hyperfine Interactions

The effect of combined magnetic and electric hyperfine interactions is shown in Figure 8. If the EFG tensor is axially symmetric ($V_{xx} = V_{yy}$) and its principal axis (V_{zz}) makes an angle γ with the magnetic field (H) axis, then a relatively simple solution exists, providing that the magnetic energy is much larger than the electric quadrupole interaction ($\mu H >> e^2qQ$); in this case the quadrupole interaction can be treated as a first order perturbation to the magnetic interaction. For a transition $\frac{3}{2} \rightarrow \frac{1}{2}$ the eigenvalues are

$$E = -g\mu_N H m_I + (-1)^{|m_I|} + 1/2 \frac{e^2qQ}{8} (3\cos^2\gamma - 1) \qquad (19)$$

When the EFG is not symmetric and the hyperfine field makes angles α, β, γ with V_{xx}, V_{yy} and V_{zz} solutions are not easily obtained unless a computer numerical analysis is used.

B. Magnetic Study

A discussion of diamagnetism and paramagnetism has been presented in detail by Muley and Boudreaux (40-42). The reader should consult books by Smart (43), Chikazumi and Charap (44), Morrish (45), Martin (46) and Turov (47) for a detailed description of the phenomenon and properties of magnetically ordered solids such as antiferromagnetic, ferrimagnetic and ferromagnetic solids.

The magnetic induction B produced in a material (in cgs Gaussian units), when placed in a magnetic field of strength H, is given by

$$B = H + 4\pi I \tag{20}$$

where I is the intensity of magnetization per unit volume in the substance. All these and related parameters are vectors. The volume magnetic susceptibility κ is given by

$$\kappa = I/H \quad , \tag{21}$$

while the per gram susceptibility χ_g is given by dividing the volume susceptibility by the density ρ of the substance. In the following sections, different types of magnetic behavior are discussed.

1. Diamagnetism

Every material has a diamagnetic susceptibility, although it is negligible in some cases because it is much weaker and masked by other types of magnetic behavior.

The effect of the interaction of an applied magnetic field on the electrons in orbitals of an atom can be understood on a qualitative basis by considering Lenz's law of electricity. When the magnetic flux enclosed by a current loop is changed, a current is induced in the loop which produces a field in opposition to the applied field. Thus the atom's electronic motion, considered as a current loop, will be changed in such a sense that a magnetic moment will be induced that opposes the applied field. Since the electron orbits may be viewed as "resistance-less," this moment will persist as long as the external field is applied. Langevin's equation for the volume diamagnetic

susceptibility of an atom is given by

$$\kappa = \frac{N_v e^2}{6m_e c^2} \sum_{i=1}^{z} \bar{r}_i^2 \quad ; \tag{22}$$

where $\bar{r}^2$ is the mean square radius of the electron's orbit when projected on a plane perpendicular to H. N_v is the number of atoms per cm^3, e is the electron charge, m_e the mass of the electron and c the speed of light.

Catalyst supports such as ZSM-5 and Silicalite (discussed under Chapter IV) are diamagnetic and their contribution to magnetization of the catalyst is obviously negligible.

2. Paramagnetism

Paramagnetism depends on the presence of a permanent magnetic moment arising from unpaired electron spins. In the absence of an externally applied field these magnetic moments average to zero. Thus, paramagnetism is the result of a system of unpaired spins reacting to an applied stress, namely the externally applied field.

It seems appropriate to proceed directly with a quantum mechanical model of a paramagnet, since the classical model does not give any extra insight, nor is it really any simpler. The magnetic moment of an atom or ion is actually determined by a more fundamental property, the angular momentum, so a brief review of some well-known rules relating angular momentum to magnetic moments will be discussed.

The orbital and spin angular momenta each have a magnetic moment associated with them, the magnetic moment relationships being given by

$$\mu_L = \frac{-|e|h}{2m_e C} L \tag{23}$$

and

$$\mu_s = -2\mu_B S \tag{24}$$

where the quantity $|e|h/(2m_e C)$ is a unit of magnetic moment equal to 0.927×10^{-20} erg/Oe; it is generally called the Bohr magneton and will be denoted by μ_B.

Figure 9 gives a vector diagram showing how L and S combine to give a total angular momentum J and how μ_L and μ_s combine to give total magnetic moment μ, where from eqs. 23 and 24

$$\mu = -\mu_B (L + 2S) \quad . \tag{25}$$

It can be seen that μ is not parallel to J because the ratios of magnetic moment to angular momentum are different in the orbital and spin cases. In the absence of an applied field, the total angular momentum J is a good quantum number; L, S, and μ, on the other hand, are constant in magnitude but precess about J. Thus, an applied field can only sense the component μ parallel to J which is called μ_J. Using properties of angular momentum and the law of cosines, we have

$$\mu_J = g \sqrt{J(J+1)}\, \mu_B \tag{26}$$

and

$$\mu_{J_z} = -g \mu_B J_z \tag{27}$$

where $g = 1 + [J(J+1) + S(S+1) - L(L+1)]/2J(J+1)$. (28)

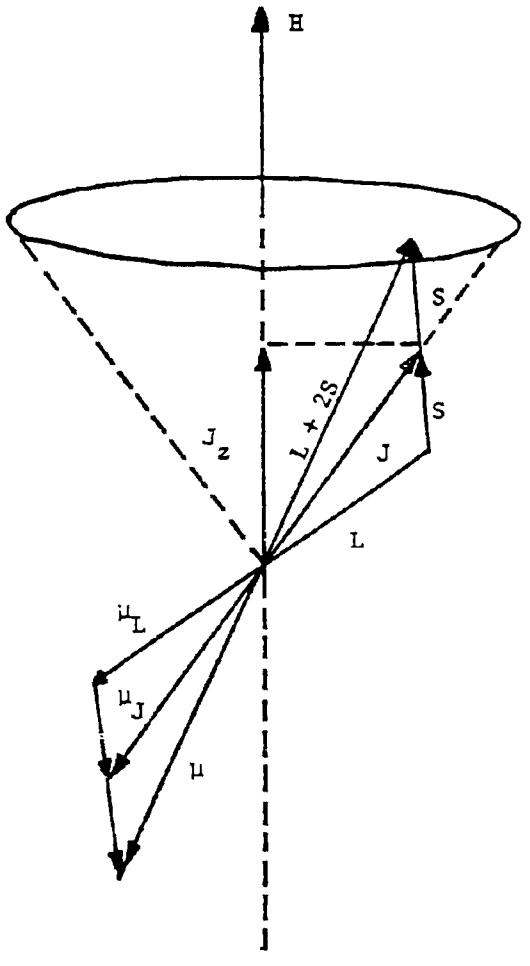

Figure 9. Vector relations between the spin, orbital and total angular moments and their associated magnetic moments.

For a detailed discussion of the above results the reader should consult an excellent monograph by Van Vleck (48).

The Hamiltonian describing the interaction of a magnetic moment μ_J and the applied field may be written as

$$\hat{H} = -\mu_J \cdot H. \tag{29}$$

Choosing H to be along the z axis we may write

$$\hat{H} = -\mu_{J_Z} H . \tag{30}$$

Combining eqs. 27 and 30 we have

$$E_m = -g\mu_B \, m \, H \tag{31}$$

where

$$m = J, J-1 \ldots -J.$$

Using methods of statistical mechamics one arrives at the following expression for the molar magnetization M of an atom or ion, namely

$$M = \frac{Ng\mu_B \sum_{m=-J}^{J} m \exp\left(g\mu_B mH/k_BT\right)}{\sum_{m=-J}^{J} \exp\left(g\mu_B mH/k_BT\right)} \tag{32}$$

where N is the number of magnetic ions or atoms per mole of substance and k_B is Boltzman's constant. When the multiplets in eq. 31 are wide compared to k_BT we obtain the molar paramagnetic susceptibility as

$$\chi_M = N \, g^2 \, J \, (J+1) \, \mu_B{}^2/3k_BT \quad , \tag{33}$$

which is known as Curie's law. When the multiplets widths are

comparable to k_BT a complicated expression is obtained, while narrow multiplets with respect to k_BT give

$$\chi_M = N g^2 \mu_B^2/3k_BT \ (L(L+1) + 4S \ (S+1)). \tag{34}$$

Weiss considered how Curie's law would be modified if there were interactions between magnetic ions, and to account for these interactions he created a fictitious field called the molecular field, given by N_wM. The modified Curie law called the Curie-Weiss law is given by

$$\chi_M = \frac{1}{T-\Theta} \tag{35}$$

where $\Theta = CN_w$ and $C = Ng^2 \ J(J+1)\mu_B^2 \ / \ 3k_B$ and is used to fit susceptibility data of magnetically ordered solids above the magnetic ordering temperatures T_N or T_C where they are paramagnetic. In section 3 the origin of the Weiss molecular field, as well as antiferromagnetism, ferrimagnetism and ferromagnetism will be discussed.

3. Magnetic Order

Magnetic order may be considered to be a special case of paramagnetism in that even in the absence of an applied field there is a spontaneous magnetization due to the Weiss molecular field. When the molecular field causes the magnetic moments in a solid to be aligned parallel to one another we have ferromagnetism, whereas antiparallel alignments of magnetic moments correspond to antiferromagnetism. Ferrimagnetism is a special case of antiferrimagnetism where there is an incomplete cancellation of antiparallel magnetic moments. For antiferromagnetic and ferrimagnetic materials it is convenient to divide the moments into sublattices. In the simplest case, a two-

sublattice model, sublattice A would have moments pointing in the +x direction while sublattice B has moments in the -x direction.

The magnetization of a paramagnet is given by

$$M(T) = N_g \mu_B J \, B_J(x) \quad , \tag{36}$$

where

$$x = Jg\mu_B H/k_B T \tag{37}$$

and

$$B_J(x) = \frac{2J+1}{2J} \coth \frac{2J+1}{2J} x - \frac{1}{2J} \coth \frac{x}{2J} \tag{38}$$

which can be derived from eq. 32. In a ferromagnetic material the field H in eq. 37 is replaced by $(H + MN_w)$ to give

$$x = (Jg\mu_B/k_B T) \; (H + MN_w) \quad . \tag{39}$$

In order to examine the spontaneous magnetization, we set $H = 0$. Rewriting eq. 36 and 39 we have

$$\frac{M(T)}{M(0)} = B_J(x) \tag{40}$$

and

$$\frac{M(T)}{M(0)} = (k_B T/Ng^2 \mu_B{}^2 J^2 N_w) \; x \; , \tag{41}$$

where $$M(0) = Ng\mu_B J \quad . \tag{42}$$

The temperature dependence of the magnetization of a ferromagnet is given by solving simultaneously eqs. 40 and 41. The temperature at

which magnetic order collapses is called T_C for a ferromagnet and T_N for an antiferromagnet.

T_C is related to N_w by

$$T_C = \frac{N^2 \mu_B J(J+1)}{3k_B} N_w \quad . \tag{34}$$

This spontaneous magnetization as a function of reduced temperature as determined by eqs. 40 and 41 is given in Figure 10 for various values of J.

Treatment of antiferromagnetic or ferrimagnetic materials proceeds in much the same way except that now there are two sublattices and two molecular field constants N_{AA} and N_{AB}. N_{AA} is the molecular field constant for coupling among ions in the same sublattice while N_{AB} is the constant for coupling between ions on sublattices A and B. The reader should consult references (41–45) for further discussion pertaining to antiferromagnetism and ferrimagnetism.

Weiss developed the molecular field model before the birth of quantum mechanics. It is now of interest to consider the concept of exchange interactions and how Weiss' molecular field is proportioned to J_e, the exchange interaction. The concept of exchange can be understood by considering a two-electron system in which each electron is on a separate ion. The Schrodinger equation may be written as

$$(\hat{H}_0 + \hat{H}')\ \psi = E\psi \ , \tag{44}$$

where the two terms in the Hamiltonian are

$$\hat{H}_o = \frac{-h^2}{2m_e} (\nabla_1^2 + \nabla_2^2) - \frac{Ze^2}{r_{a1}} - \frac{Ze^2}{r_{a2}} \tag{45}$$

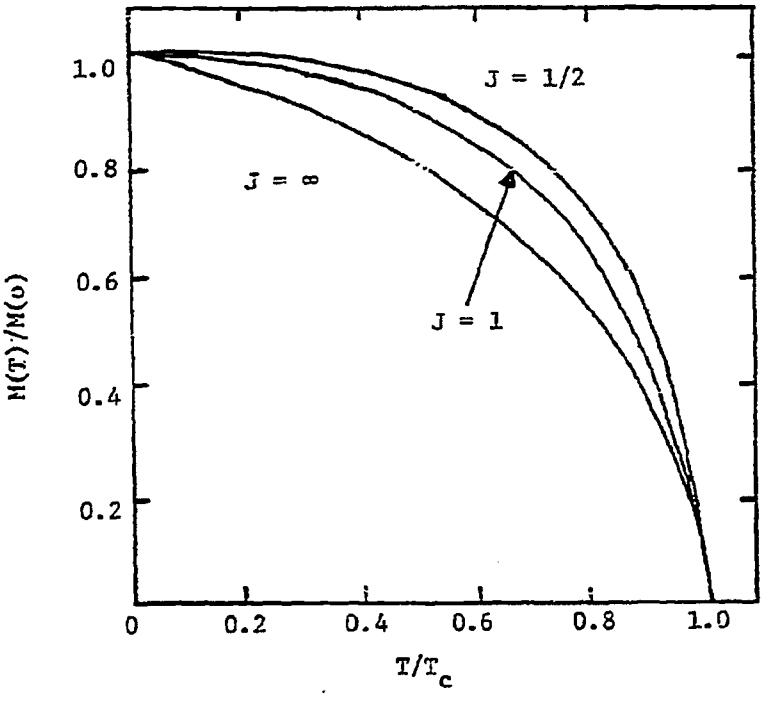

Figure 10. The spontaneous magnetization as a function of reduced temperature for J = 1/2, 1, ∞. The value of J = ∞ corresponds to the classical case where J can take on an infinite number of values.

and

$$\hat{H}' = \frac{Ze^2}{r_{ab}} + \frac{e^2}{r_{12}} - \frac{Ze^2}{r_{12}} - \frac{Ze^2}{r_{b1}} - \frac{Ze^2}{r_{a2}} \tag{46}$$

The subscripts 1 and 2 refer to the two electrons, and subscripts a and b refer to the two ions, each with effective nuclear charge Z.

Because of the indistinguishability of electrons the two orbital wave functions are

$$\psi_{\pm} = \frac{1}{\sqrt{2 \pm S^2}} [\phi_a(1)\phi(2)_b \pm \phi_a(2)\ \phi_b(1)] \quad , \tag{47}$$

where ϕ_i are eigenfunctions of the atomic Hamiltonian and S is the overlap integral. In the absence of the exchange interactions (represented by H'), the energy of the two-electron systems is just $2E_o$. In the presence of exchange interactions it is found that

$$E_+ = 2E_o + \frac{J_e + K}{1 + S^2} \quad , \tag{48}$$

$$E_- = 2E_o + \frac{K - J}{1 - S^2} \quad , \tag{49}$$

where

$$J_e = \langle \phi_a(1)\ \phi_b(2) | \hat{H}' | \phi_a(2)\phi_b(1) \rangle \tag{50}$$

and

$$K = \langle \phi_a(1)\ \phi_b(2) | \hat{H}' | \phi_a(1)\phi_b(2) \rangle \tag{51}$$

K is the electrostatic energy between atoms, and is called the Coulomb energy and J_e is the exchange energy. When the spin properties are added to the wave functions $\psi_{\pm}$ we now have wave functions α_S and α_T

which have their spins antiparallel or parallel, respectively, and are called singlet or triplet states. The singlet and triplet states differ in energy because their orbital functions are different. In the zero overlap approximation E_+ and E_- differ by $2J_e$. If J_e is a positive number the triplet state lies lowest and the interaction is said to be a ferromagnetic one. However, if J_e is negative the singlet state lies lowest and the interaction is antiferromagnetic.

The exchange Hamiltonian describing the exchange interactions in solids is given by

$$\hat{H} = -2 \sum_j J_{ij} S_i S_j \tag{52}$$

which is known as the Heisenburg Hamiltonian. To summarize the above mathematical treatment of exchange interactions and the consequences of the Pauli principle, the exchange force may be thought of in the following simplistic way. In the triplet state the motions of the electrons are correlated so that they avoid one another as much as possible, while in the singlet state they attract each other. That is, they move as if they were under the influence of a force that is repulsive for parallel spins and attractive for antiparallel spins. This force is called the exchange force since it has its origin in the symmetry requirements on the wave function under the exchange of indistinguishable particles. The exchange force is strictly a quantum mechanical phenomenon with no classical analog.

The Weiss molecular field constant has its origin in exchange force and for a ferromagnet,

$$N_w = 2ZJ_e/Ng^2\mu_B^2 \tag{53}$$

Exchange interactions in solids are usually determined by measurement of T_c or T_N and the Curie-Weiss constant θ in eq. 35 from high temperature susceptibility data. Smart (43,49) gives an excellent account of the various methods employed in determining exchange interactions in solids from experimental data.

4. Superparamagnetism

The phenomenon of magnetically ordered materials such as (a) ferro-, (b) ferri- and (c) antiferromagnetic materials is very well known. The first two consisting of multidomain particles show a definite Curie point in magnetization (σ) vs. temperature (T) curves. Beyond this temperature the material changes over to normal paramagnetism. In the case of (c) that is antiferromagnetism one encounters the Neél temperature (T_N) beyond which the material again becomes paramagnetic.

Now, if subdomain particles ($\gtrsim$ 20 nm) of the above mentioned materials are considered each such particle will consist of several hundred or thousand uncompensated species with a net Bohr magneton number of $\sim 10^3$ to 10^4. If there is no magnetic interaction (ordering) between such particles, they are said to behave superparamagnetically. This means that particles have enough thermal energy to be randomized independently of each other; whereas below a certain temperature called the blocking temperature, (T_B), they are stable enough and may show small hysteresis. The reader should consult references (50-57) for detailed description of the properties of superparamagnetism.

Real particles are never truly isotropic. In general, the anisotropy energy (K') amongst other factors is proportional to the

volume of the particle (50). Suppose an assembly of uniaxial particles has been brought to some initial state of magnetization M_i by an applied field, and the field is then turned off at time t = 0. Some particles in the assembly will immediately reverse their magnetization because of thermal energy, and the magnetization will begin to decrease. The rate of decrease at any time will be proportional to the magnetization at that time and to the Boltzmann probability factor $e^{-K'\bar{V}/kT}$. Therefore,

$$-\frac{dM}{dt} = f_o M\, e^{-K'\bar{V}/kT} = \frac{M}{\tau} \tag{54}$$

where proportional constant f_o is a frequency factor of the order of $10^9\ s^{-1}$, K' the anisotropy constant, $\bar{V}$ the volume of the particles, k the Boltzmann constant, and τ the relaxation time. We rearrange the terms and integrate to obtain

$$M_r = M_i \exp\ (-t/\tau) \tag{55}$$

and

$$\tau^{-1} = f_o \exp(-K\bar{V}/kT) \tag{56}$$

where M_r is the remanence at time t. The value of τ is strongly dependent on the particle volume $\bar{V}$ and the temperature T since both are in the exponent.

It is generally difficult to separate out the superparamagnetic contribution in a mixture of ferromagnetic and superparamagnetic system. Although this has been done by Everson et al. (58) with respect to studies in Ni on Al_2O_3 catalyst, little work has been done on Fe catalysts. The delineation of the superparamagnetic and ferro-

magnetic contribution is difficult using static measurements; the elegance of Mössbauer spectroscopy lies in the fact that superparamagnetic particles can be detected usually as a doublet in the presence of more complex spectra arising from magnetically ordered materials. The doublet from superparamagnetic particle is dependent on the thermal relaxation of such a particle; it can be elucidated by studying the Mössbauer spectroscopy at cryogenic temperature. Then by knowing reasonable values for K' (anisotropy constant) it is possible to obtain the average particle size ($\bar{V}$) of the superparamagnetic particle from eq. 56. This approach has been followed by many workers [cf. Collins et al. (59) and references cited therein].

III. EXPERIMENTAL PROCEDURES

A. Preparation of Samples

The zeolites ZSM-5 and Silicalite were prepared according to procedures described in the literature (60,61). Both are medium pore zeolites with effective diameters between those of zeolite Linde type A and faujasite and have similar crystal structures (62,63). The pore structure consists of a three-dimensional system of intersecting channels defined by 10 rings of oxygen ions in all three directions. The elliptical, straight channels of cross-section 5.7 Å x 5.1 Å along the b axis and near-circular zig-zag channels of diameter 5.4 Å along the a-axis are interconnected. The Si/Al ratio in ZSM-5 can be varied from 3 to 100, but Silicalite has no Al sites. Hence it appears that Silicalite is the limiting form of ZSM-5 when the Al concentration is near to zero.

The transition metal component (Fe and/or Co) was introduced by gradually adding the metal nitrate solution to the zeolite until incipient wetness was reached. The impregnation with the metal nitrate solution was carried out for an hour under vacuum in order to enable the nitrate solution to enter the pores of the zeolite. The material was initially dried with constant stirring over a boiling water bath, and further dried in air at 110°C for 12 hours.

The zeolite impregnated with Fe or Fe + Co was reduced in flowing H_2 at 450°C for 24 hours. It was then carbided in flowing synthesis gas at 250°C for 24 hours to yield the active catalyst. The catalysts were tested for synthesis gas conversion in both a fixed bed microreactor and a Berty (continuous flow stirred tank) reactor in PETC.

For Mössbauer studies, all the samples except the used catalysts were prepared separately under the conditions described above. In the ensuing discussion such samples will be described variously as (a) freshly impregnated, (b) reduced, (c) carbided and (d) used catalysts.

Samples for Mössbauer study were first ground to about 200 mesh (100 μm) in a dry-box flowing with inert gas when it was necessary. They were then weighed so that the thickness of the absorber consisted of about 30 mg/cm^2 of sample in order to prevent line broadening due to a thick absorber. Samples were spread onto an aluminum foil (99.9999% purity) of 0.025 mm thickness purchased from Alfa Products, Danvers, MA. The area of the sample was about 4 cm^2, so that 120 mg of sample was used for Mössbauer measurements.

B. Catalysis Reaction Studies

These were carried out on the above samples at the Pittsburgh Energy Technology Center, Pittsburgh, PA. A summary of important results is given in Chapter IV.

C. Mössbauer Apparatus

A block diagram of the Mössbauer spectrometer and its associated electronics is shown in Figure 11. The Mössbauer drive unit and a transducer operating in a constant acceleration mode (Nuclear Science and Engineer Corp.) was used with a 75 mCi Co^{57} source in Rh matrix. The 14.4 KeV γ-rays were detected using a Reuter-Strokes gas proportional counter containing 90% krypton and 10% methane. A typical γ-radiation spectrum in the low-energy region is shown in Figure 12. In subsequent work on Austin Associates Spectrometer with a helium-neon

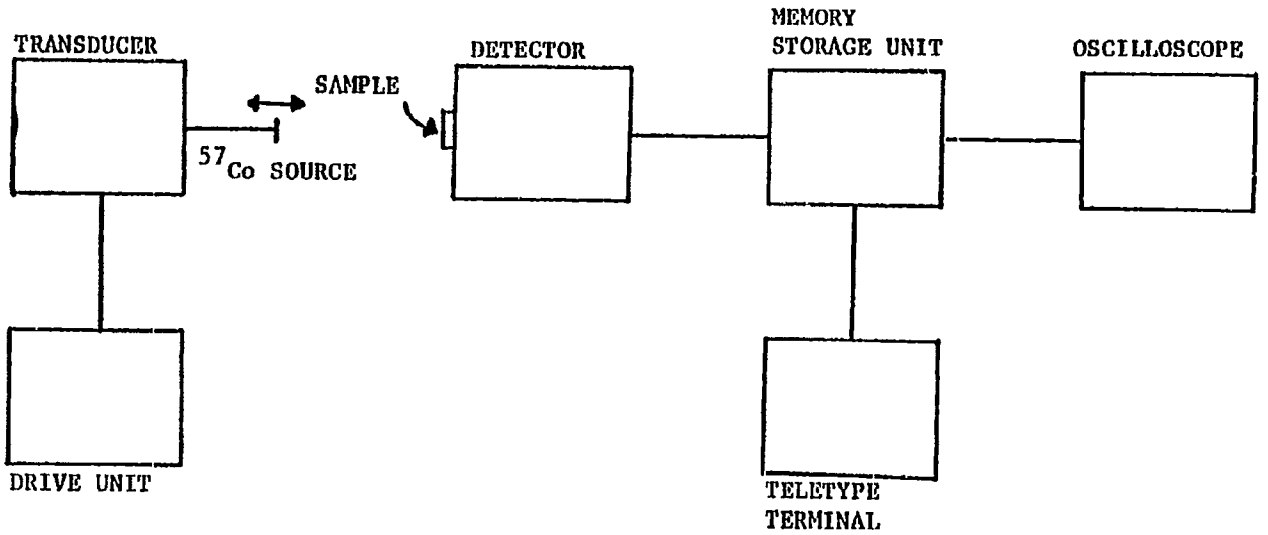

Figure 11. Block diagram of the Mössbauer spectrometer.

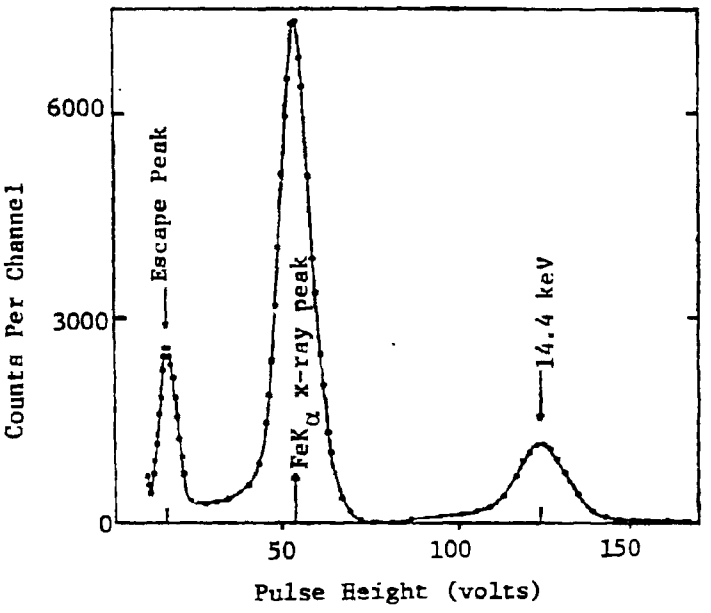

Figure 12. Pulse height distribution for the 14 keV γ-radiation and the iron K x-radiation using a krypton filled proportional counter.

laser interferometer (for absolute velocity calibration) was used. The other electronic units consisted of a multichannel analyzer (Nuclear Data-100) with 1024 channels, preamplifier, high voltage supply, and analog-to-digital converter (Nuclear Date-570). The teletype terminal was manufactured by the Teletype Corporation.

All Mössbauer measurements below room temperature were performed using a Model LT-3-110 liquid transfer "Heli-Tran." The "Heli-Tran" was used in conjunction with an APD-E digital temperature controller, both of which were made by Air Products and Chemicals, Inc., Allentown, PA. The aluminum foil containing the sample was attached to a special sample holder supplied by Air Products and Chemicals, Inc., which was then screwed into the tip of the cold finger. The sample temperature could be maintained to ±0.10 K with this cyrostat. The thermalcouple was calibrated by Air Products and Chemicals, Inc. For a detailed description of the theory and method of operation of the cyrostat, the reader should consult several excellent manuals written by Air Products and Chemicals, Inc.

D. Calibration and Measurements

It was necessary to calibrate the spectrometer with a standard that could be used for the comparison of experimental data. The velocity of the Mössbauer drive unit was set so that all peaks of the iron spectrum were well contained within the 512 channels of the multichannel analyzer. Calibration was performed using a natural Fe foil supplied by the National Bureau of Standards, Washington, DC for which six line positions occur at 398, 341, 283, 236, 179, and 122 channels corresponding to +5.2034, +2.9651, 0.7248, -0.9528, -3.1931, and =5.4314 mm/sec relative to Co^{57} in rhodium. A graph of these known

iron peak velocities versus peak channel numbers was then plotted (Figure 13), and a straight line fitted by least squares method was obtained. The linearity of the Mössbauer drive was found to be within ±0.5%. The slope of the line gives the velocity increment per channel (mm/sec/channel) so that any channel number could be converted to a velocity scale in mm/sec.

E. Analysis of Mössbauer Data

The Mössbauer data were obtained from the spectrometer in the form of a punched paper tape and also printed on the teletype and recorded on the plotter. A computer program was used to convert the contents of the paper tape onto computer cards. A least squares computer program was used to fit the Mössbauer spectra, assuming Lorentzian line shapes. The program was capable of varying the line widths, peak height ratios, intensities and number of hyperfine interactions to obtain the best fit. A subroutine for the calculation of X square and MISFIT developed by S. L. Ruby (64) of the Argonne National Laboratory was also included in the main computer program to compute the quality of the fitting obtained. Calcomp-Compatible Subroutines were then used to plot either with number of counts versus channel numbers or relative transmission versus velocities.

F. Characterization by X-ray Diffraction

An automated X-ray powder diffractometer (Philips APD 3600/01) with $CuK\alpha$ radiation was used for structure and orientation determinations. Samples were ground and spread onto glass microscope slides (25 x 40 x 1 mm) in a dry-box flowing with inert gas. Whenever

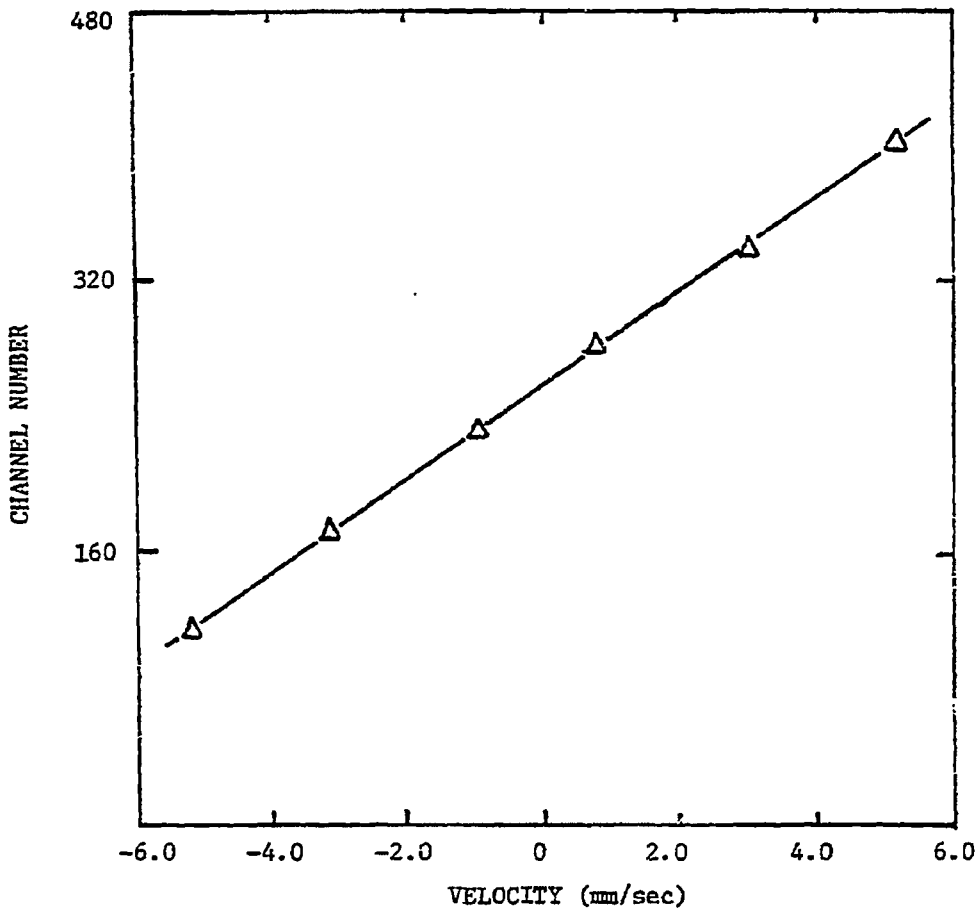

Figure 13. Calibration plot of velocity versus channel number for the six peaks of ^{57}Fe. The slope of this line gives the velocity calibration (mm/sec/channel)

necessary Collodion-acetone mixture was used to make the sample adhere to the glass slides. A low scanning speed of 1° per minute was used to determine the average crystallite size.

Typical X-ray powder patterns of ZSM-5 and silicalite are shown in Figure 14. Table 1 presents the d-spacing calculated from ZSM-5 X-ray diffraction pattern.

G. Magnetic Measurements

A Faraday Cahn RH electrobalance was used to measure the magnetization and susceptibility in the temperature range 78 to 1000 K, and in applied magnetic fields up to 20 KOe. For a detailed description of the Faraday technique the reader should consult an excellent monograph by Mulay (65).

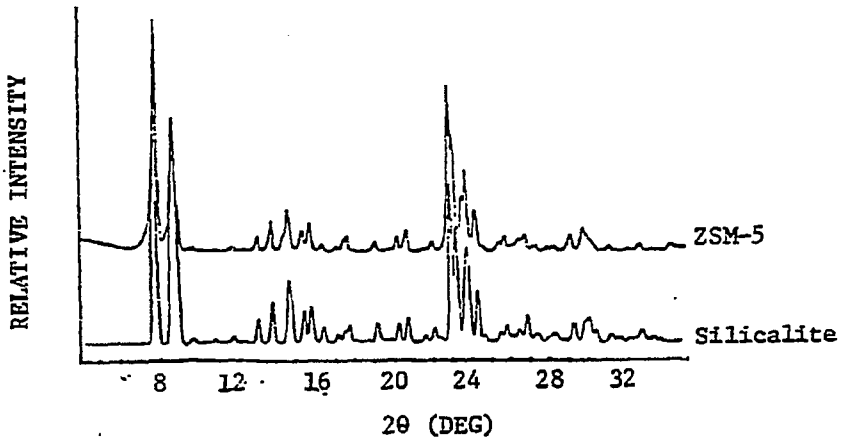

Figure 14. X-Ray diffraction patterns of ZSM-5 and Silicalite

TABLE 1. Interplanar d-Spacing (Å) of ZSM-5

Interplanar spacing d (Å)	Relative intensity
11.1	Strong
10.0	Strong
7.4	Weak
7.1	Weak
6.3	Weak
6.0	Weak
5.6	Weak
5.0	Weak
4.6	Weak
4.3	Weak
3.9	Very strong
3.7	Strong
3.0	Weak
2.9	Weak

IV. RESULTS AND DISCUSSION

A. General Introduction

This chapter is based on a manuscript entitled "Mössbauer and Magnetic Studies on Bifunctional Medium Pore Zeolite-Fe Catalysts Used in Synthesis Gas Conversion." This manuscript will shortly appear in "Recent Advances in the Chemical Applications of Mössbauer Spectroscopy" Eds. G. Shenoy and J. G. Stevens, to be published in the Monograph Series of the American Chemical Society. The manuscript reflects the work which was presented at a special symposium on Mössbauer Spectroscopy, held in Houston, TX, during March 1980, sponsored by the 179th National Meeting of the American Chemical Society. In section B some of the earlier description of experimental techniques, etc., (Chapter III) is again succinctly summarized.

B. Mossbauer and Magnetic Studies on Bifunctional Medium Pore Zeolite-Fe Catalysts Used in Synthesis Gas Conversion

1. Introduction

The catalytic conversion of coal-derived synthesis gas ($CO + H_2$) to gasoline range hydrocarbons and olefins using bifunctional zeolite catalysts (66-68) is of much current interest. The medium pore (dia $\sim$ 6Å) zeolite ZSM-5 in combination with Fe (66,67) or with Fe-Co (68) was shown to yield a high fraction of aromatics in the product, resulting in a favorable octane number (>80). It was indicated (68) that the bimetallic Fe-Co on ZSM-5 could alter the product selectivity, mainly in reducing the "shift" conversion of $CO + H_2O$ to CO_2, from the high shift yields of Fe on ZSM-5. The aromatics in the product decreased by the addition of cobalt to iron in the zeolite (68).

In contrast to ZSM-5, Silicalite lacks aluminium although the two appear to possess similar crystal structures (62,63). They crystallize with the orthorhombic space group Pnma or $Pn2_1a$ with a = 20.1 Å; b = 19.9 Å; c = 13.4 Å. The framework structure consists of five membered rings of Si(Al)-O tetrahedra. The pore structure (Figure 15) consists of intersecting channels defined by 10 rings of oxygen atoms. The elliptical, straight channels of cross-section 5.7 Å x 5.1 Å along the b-axis and circular zig-zag channels of diameter 5.4 Å interconnect the straight channels.

While the Si/Al ratio in ZSM-5 can be varied from 3 to over 100, Silicalite has essentially no Al. Hence it appears that Silicalite is the limiting form of ZSM-5 when the Al concentration is vanishingly small. A comparison of the properties of ZSM-5 and Silicalite is shown in Table 2.

Owing to the absence of cations which can be exchanged with protons, Silicalite has no acidity, while HZSM-5 is a highly acidic zeolite. Recent investigations (68) have shown that the difference in selectivity for synthesis gas conversion by ZSM-5 (Fe) and Silicalite (Fe) catalysts results from the above mentioned difference in acidity. The main influence was on the production of aromatics and olefins; the former were dominant with the acidic ZSM-5 (Fe) catalyst and the latter with the non-acidic Silicalite (Fe) catalyst.

Mössbauer and magnetic investigations were conducted to determine the state of Fe and Fe-Co in the zeolite catalyst at different stages of catalyst preparation and use. Among the several aims of the investigation, were the determination of:

(a) the valence state of the transition metal in the freshly impregnated state,

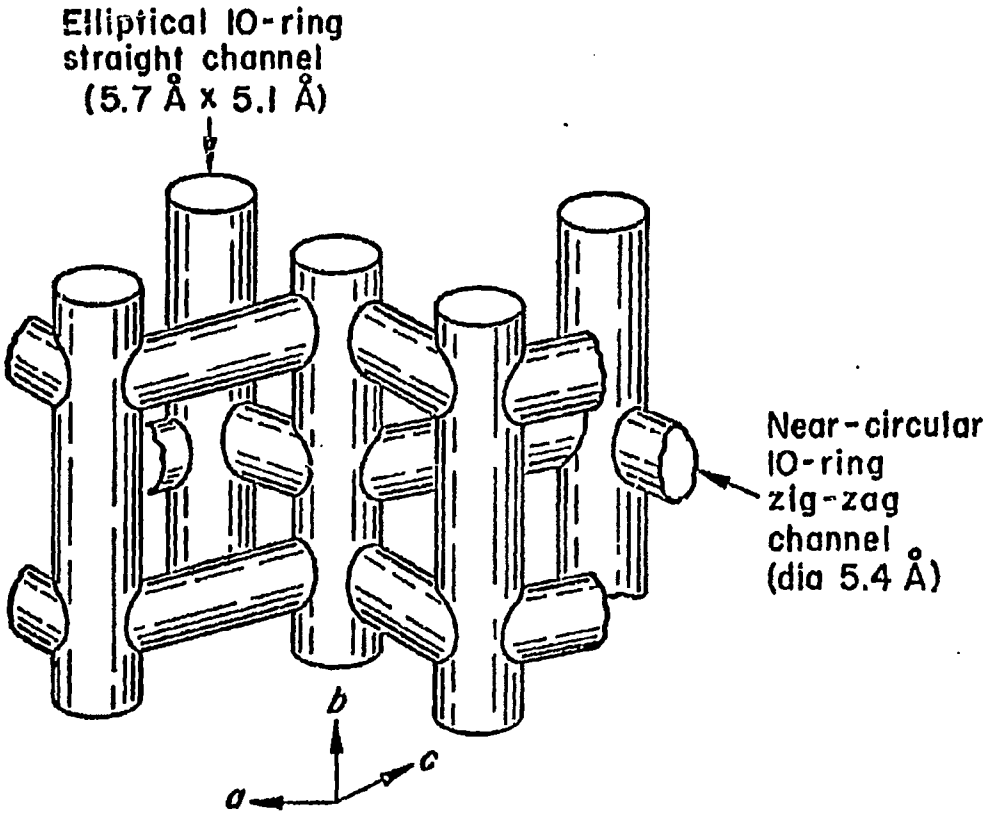

Figure 15. Possible model of the pore structure of ZSM-5 and Silicalite.

TABLE 2. Comparison of ZSM-5 and Silicalite

	ZSM-5	Silicalite
1. Composition	$Na_x(AlO_2)_x(SiO_2)_{100-x}$ $x = 1$ to 25	SiO_2 $x = 0$
2. Ion Exchange properties	Present $Na^+ \xrightarrow{EXCH} NH_4^+ \xrightarrow{Calcine} H^+$	Absent
3. Crystal Structure	Orthorhombic a = 20.1 Å b = 19.9 Å c = 13.3 Å	Orthorhombic a = 20.06 Å b = 19.80 Å c = 13.36 Å
4. Pore Structure	Straight channels along b-axis Zig-zag along a-axis. Pore diameter = 6 Å.	Same as ZSM-5
5. Sorption of H_2O	Low for Si content	Low
6. Thermal Stability	Increases with Si content	High

(b) the extent of reduction on exposing to H_2,

(c) the active catalytic species after carbiding with synthesis gas,

(d) the species present in the used catalyst, and

(e) in the case of Fe-Co, the possible formation of bimetallic or alloy clusters and its influence on the selectivity of the catalyst.

2. Experimental

ZSM-5 and Silicalite were prepared using methods described in the literature (60,61). X-ray powder diffraction patterns revealed no phases other than ZSM-5 or Silicalite. The metal component was introduced by gradually adding the metal nitrate solution to the zeolite until incipient wetness was reached. The impregnation with the metal (Fe or Fe + Co) nitrate solution was carried out for an hour under vacuum in order to enable the nitrate solution to enter the pore of the zeolite. The material was initially dried with constant stirring over a boiling water bath, and further dried in air at 110°C for 12 hours. The amount of Fe and Co in the samples was determined by standard wet chemical techniques and atomic absorption.

The zeolite impregnated with Fe or Fe + Co was reduced in flowing H_2 at 450°C for 24 hours. It was then carbided in flowing synthesis gas at 250°C for 24 hours to yield the active catalyst. The catalysts were tested (68) for synthesis gas conversion in both a fixed bed microreactor and a Berty (continuous flow stirred tank) reactor. For catalytic testing, the above steps on the metal impregnated zeolite were all carried out in the reactor. For Mössbauer studies, all the

samples except the used catalysts were prepared separately under the conditions described above. In the ensuing discussion such samples will be described variously as (a) freshly impregnated, (b) reduced, (c) carbided and (d) used catalysts. The last mentioned was taken from the reactor after their use ranging from 280°C to 320°C. X-ray diffraction studies were carried out on the samples after steps (a) and (d) above.

The apparatus used for Mössbauer spectroscopy and magnetic measurements is described separately under the corresponding sections.

3. Results and Discussion

A. Mössbauer Studies

The Mössbauer Spectra of Catalysts listed in Table 3 were recorded utilizing a conventional constant acceleration spectrometer made by Nuclear Science and Engineering Corp. and Nuclear Data ND-100 Multichannel Analyzer in MCS mode. The spectra were calibrated with a standard NBS iron foil. The parabolic background observed in the spectra arose from the geometry of the Mössbauer set up. A least squares program fitting, in progress, has justified our interpretations. The spectra were recorded at room temperature using a 75mCi Co^{57} in Rh matrix. The spectra were analyzed, in general, on the basis of the studies on carbides by Raupp and Delgass (27).

The Mössbauer spectra of the different catalysts were recorded at various stages; viz. (a) after impregnation with $Fe(NO_3)_3$, (b) on reduction in H_2 at 450°C for 24 hrs, (c) on carbiding in 1:1 H_2/CO synthesis gas at 250°C for 24 hrs and (d) finally after utilization of the catalyst in the conversion of the synthesis gas to gasoline range of hydrocarbons. The spectra have revealed the existence of various

TABLE 3. Summary of Mossbauer Results of Various Catalysts

Sample No.	Sample	State	Remarks
M1	ZSM-5 (14.7% Fe)	Reduced	Fe-metal and small amount of an oxide ($\alpha - Fe_2O_3$)
M2	ZSM-5 (14.7% Fe)	Carbided	Fe_5C_2, and Fe_3C
M3	ZSM-5 (14.7% Fe)	Used	Fe_5C_2, Fe_3C and Fe_3O_4 Fe_5C_2 has been relatively reduced as compared to that in Sample No. (2)
M4	ZSM-5 (5.4% Fe+1.3% Co)	Reduced	Fe-Co alloy
M5	ZSM-5 (5.4% Fe+1.3% Co)	Carbided	Fe_5C_2, Fe_3C and a strong doublet
M6	ZSM-5 (5.4% Fe+4.5% Co)	Used	Fe-Co alloy Co seems to have inhibited the formation of carbides.
M7	Silicalite (13.6% Fe)	Fresh	Strong doublet corresponding to Fe^{3+}
M8	Silicalite (13.6% Fe)	Used	Fe_5C_2 and Fe_3C
M9	Silicalite (4.4% Fe+3% Co)	Reduced	Fe-Co alloy
M10	Silicalite (4.4% Fe+3% Co)	Used	Fe_5C_2, Fe_3C and a strong doublet Fe_5C_2 and Fe_3C are considerably small compared to those observed in Sample No. 9. Presence of Co seems to have inhibited the formation of carbides.

phases, formed at different stages and have given clues to the nature of the active component(s), responsible for the efficient conversion of synthesis gas into gasoline.

The spectrum of a fresh catalyst, in general, consisted of a doublet with an isomer shift of about +0.35 mm/sec and a quadrupole splitting of about 0.75 mm/sec which indicate that the valence state of iron in the starting material is Fe^{3+}. A typical spectrum for a fresh catalyst of Silicalite impregnated with 13.6% Fe using $Fe(NO_3)_3$ is shown in Figure 16.

As discussed in a later section the magnetization (M) versus magnetic field (H) measurements on the fresh catalyst gave a magnetic moment of about $5.96\mu_B$, which further confirmed that the iron ion is a high-spin Fe^{3+} state. It should be noted that the magnitude of the quadrupole splitting and isomer shift significantly depend upon the nature of the support used and the size of the iron particles (18).

The spectra of a reduced catalyst consisted of a six-line pattern corresponding to mostly Fe-metal, and indicated the presence of a small quantity of an oxide. If the catalyst contained only Fe; on the other hand, the spectrum of the catalyst consisting of both Fe and Co clearly indicated the formation of a Fe-Co alloy on reduction. The spectrum of reduced ZSM-5 containing 14.7% Fe is shown in Figure 17. The spectrum essentially corresponds to that of metallic iron. However there is a small amount of unreduced iron in the form of an oxide, probably α-Fe_2O_3. The reduction in this case is about 85%. This is also confirmed by the magnetization measurements, which indicated ~15% lowering in the observed saturation magnetization of iron.

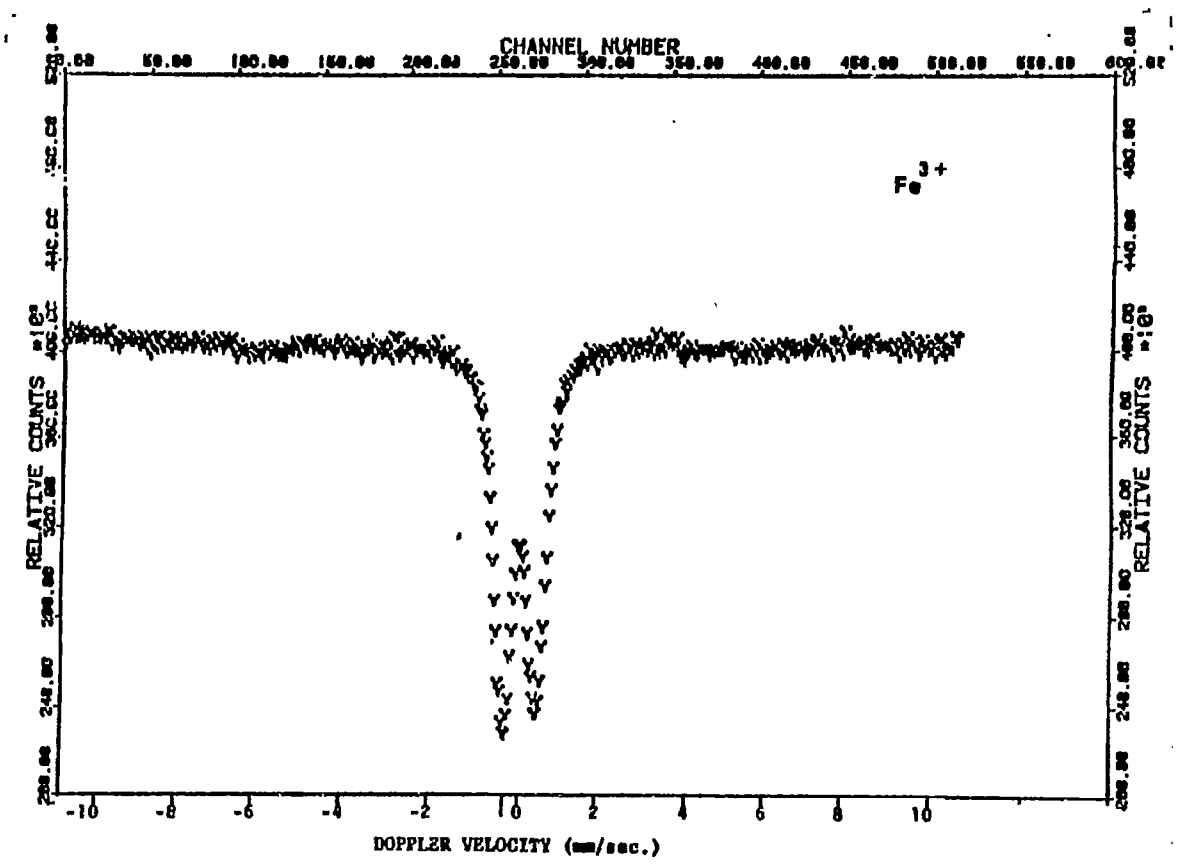

Figure 16. Mössbauer spectrum of Silicalite impregnated with 13.5% Fe using $Fe(NO_3)_3$

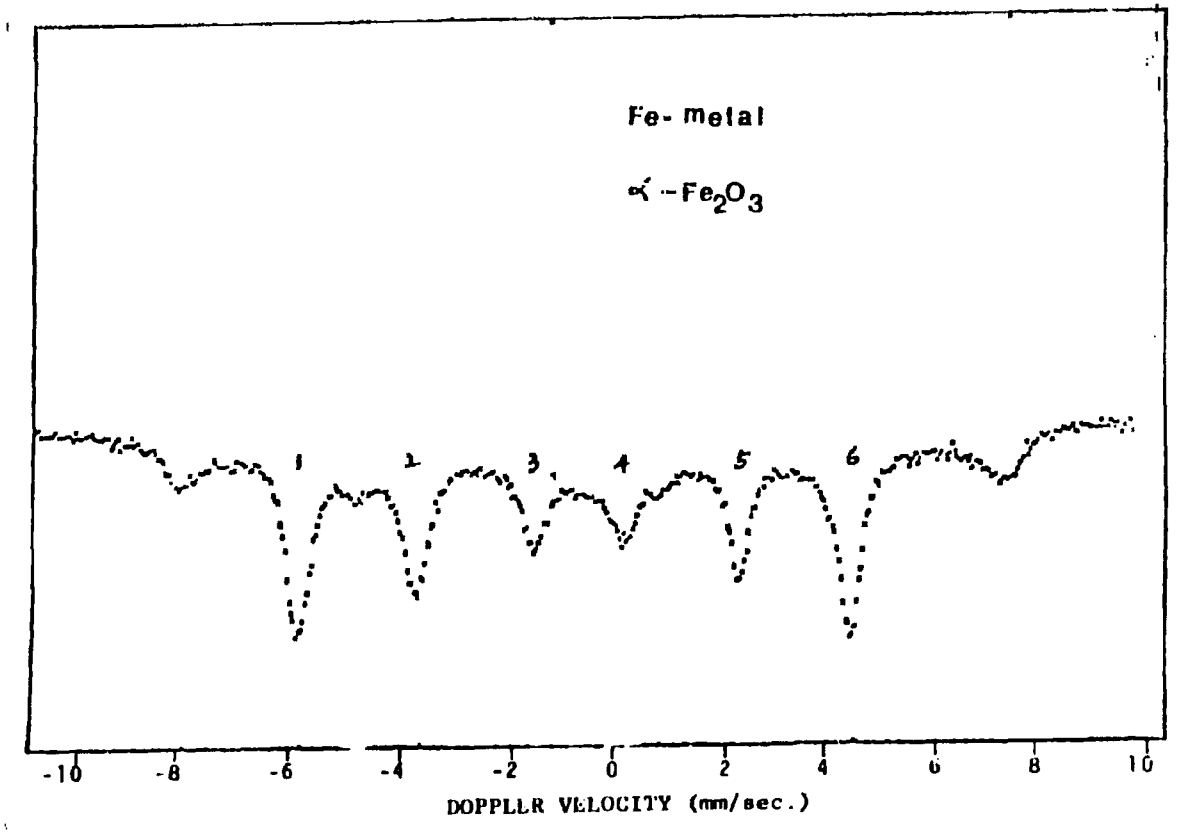

Figure 17. Mössbauer spectrum of reduced ZSM-5 (14.7% Fe)

The spectrum of reduced ZSM-5 containing 5.4% Fe and 1.3% Co, shown in Figure 18, revealed a six-line pattern corresponding to an average internal magnetic field of about 340 kOe and indicated the formation of an Fe-Co alloy.

A typical spectrum of reduced Silicalite containing 4.4% Fe and 3.0% Co is shown in Figure 19. The spectrum consists of a well defined six-line pattern corresponding to an internal magnetic field of 345±3 kOe which is much larger than 330 kOe, expected for metallic iron. Secondly, the isomer shift observed is 0.18 mm/sec, with respect to Fe-metal which indicates that the electron density at the Fe-nucleus is smaller in the Fe-Co alloy as compared to that in Fe-metal. This decrease in the electron density in the Fe-Co alloy is consistent with the experimental results reported by Van der Woude and Sawatsky (69). The formation of a Fe-Co alloy is further supported by the magnetization measurements on this catalyst, which indicated a magnetic moment, intermediate between the moments corresponding to Fe and Co.

The spectra of carbided catalysts consist of superposition of at least two apparent six-line patterns corresponding to at least two different Fe-C phases. A typical spectrum of caribded ZSM-5 with 14.7% is shown in Figure 20. This spectrum represents the presence of Hagg carbide (Fe_5C_2) and cementite (Fe_3C). The former has 3 inequivalent Fe sites, whereas, the latter has only one. The possibility of the presence of small quantities of less stable ε' and ε carbides ($Fe_{2.2}C$ and Fe_2C) cannot be ruled out. A doublet due to Fe^{3+} was not apparent in Figure 20; further low temperature studies are in progress to discern any superparamagnetic behavior.

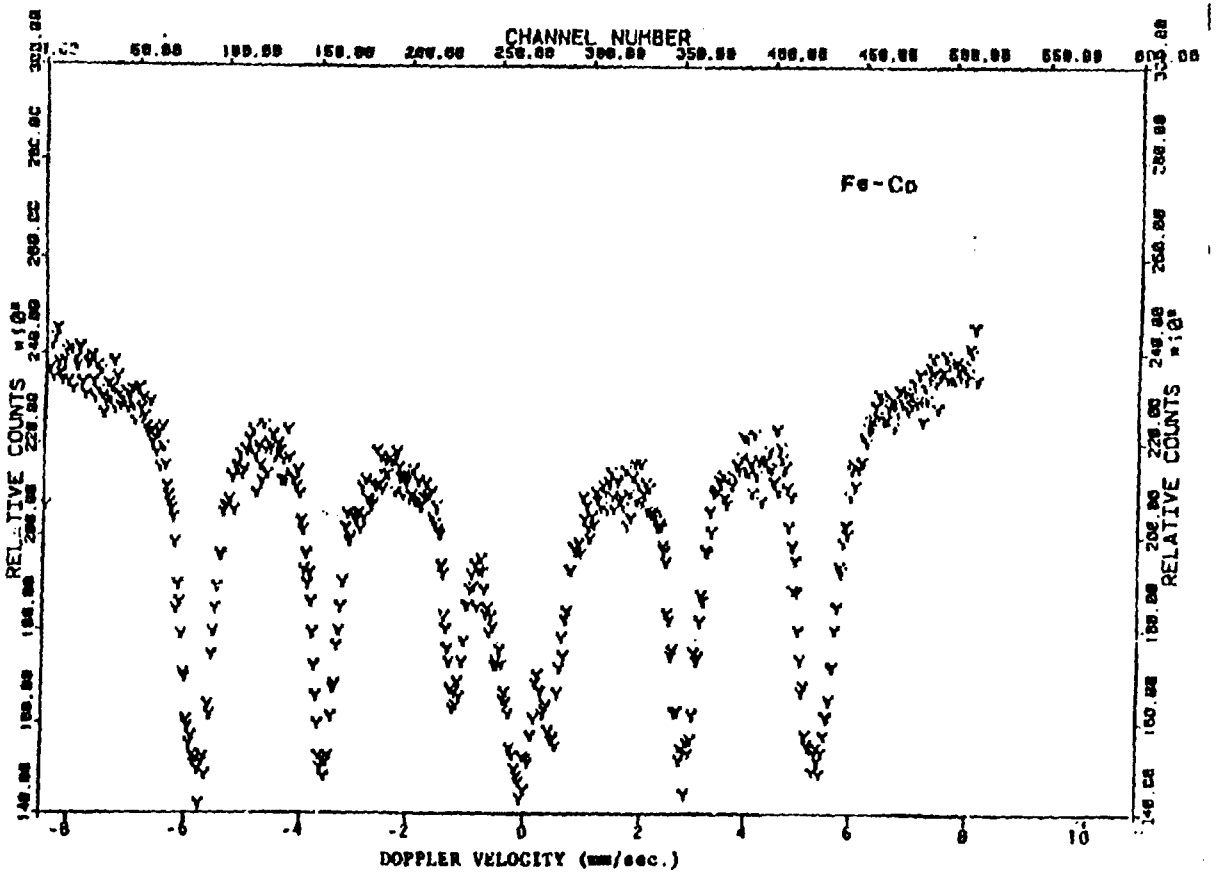

Figure 18. Mössbauer spectrum of reduced ZSM-5 (5.4% Fe, 1.3% Co)

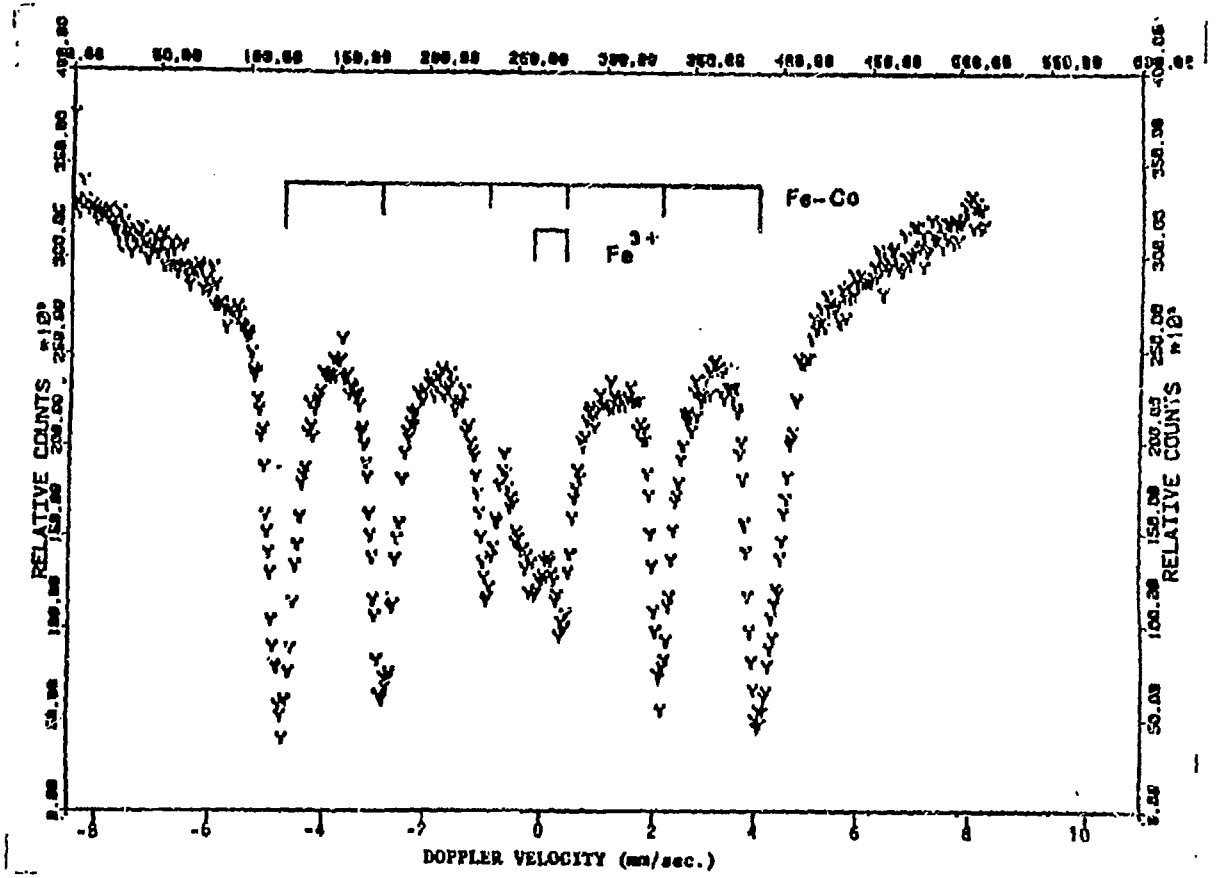

Figure 19. Mössbauer spectrum of reduced Silicalite (4.4% Fe, 3% Co)

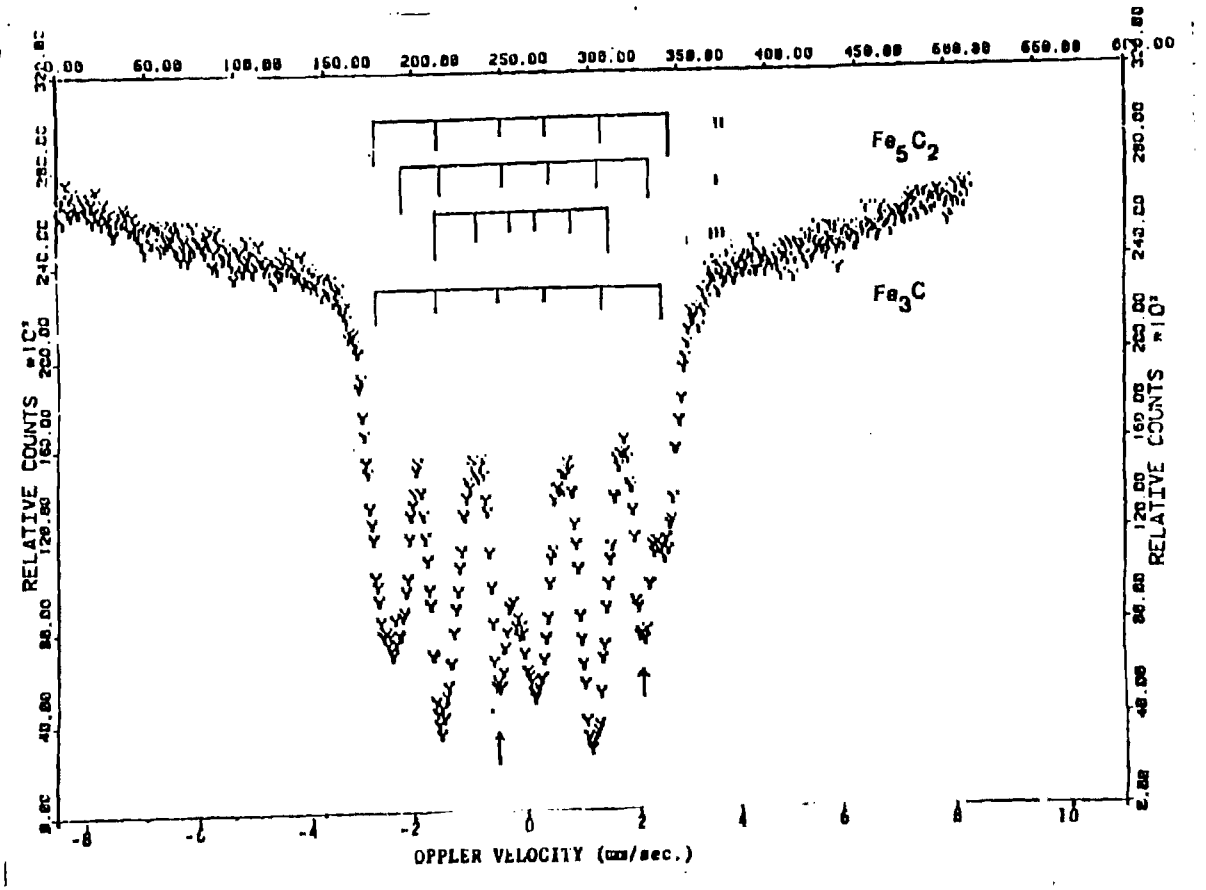

Figure 20. Mössbauer spectrum of carbided ZSM-5 (14.7% Fe)

The spectrum of carbided ZSM-5 containing 5.4% Fe and 1.3% Co, shown in Figure 21, indicates the presence of both Fe_5C_2 and Fe_3C besides a strong doublet. Apparently less amounts of carbides seem to have been formed in this catalyst as compared to those containing no Co. It appears that the presence of Co has somewhat inhibited the formation of carbides. The doublet may be due partly to superparamagnetic behavior. Similar spectra have also been observed in the case of Silicalite-based catalysts as well. Further low temperature studies are underway to identify the nature of the doublet.

The spectra of used catalysts are in general very complicated and seem to consist of three or more magnetically split hyperfine spectra. A typical spectrum of used ZSM-5 with 14.7% Fe is shown in Figure 22. This spectrum can be explained in terms of the presence of Hagg Carbide, cementite, and Fe_3O_4. It is noteworthy that the cementite content is relatively increased at the expense of the Hagg Carbide in the used catalyst as compared to that found in the carbided catalyst. [See the lines marked by arrows in Figure 20 and Figure 22.]

The spectrum of used ZSM-5 with 5.6% Fe and 4.5% Co shown in Figure 23, consists of a six-line pattern corresponding to an internal magnetic field of 344±3 kOe and an isomer shift of +0.15 mm/sec with respect to Fe-metal and appears to indicate the formation of an Fe-Co alloy. It is to be noted that the carbides, which were present in the case of used ZSM-5 containing only Fe, are surprisingly absent in this case. Once again, the presence of a large amount of Co appears to inhibit the formation of carbides in these samples. The X-ray powder patterns showed the presence of a bcc Fe-Co alloy phase in addition to the ZSM-5 phase.

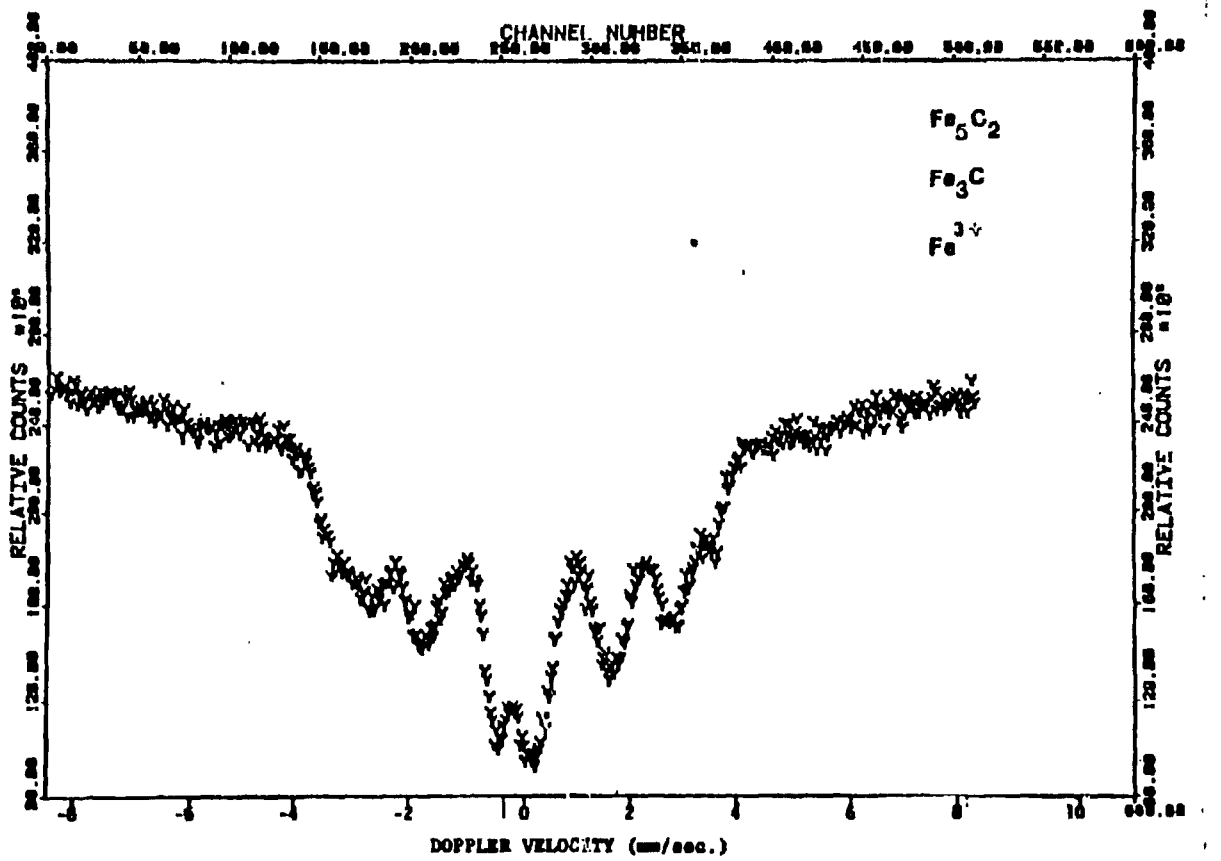

Figure 21. Mössbauer spectrum of used ZSM-5 (5.4% Fe, 1.3% Co)

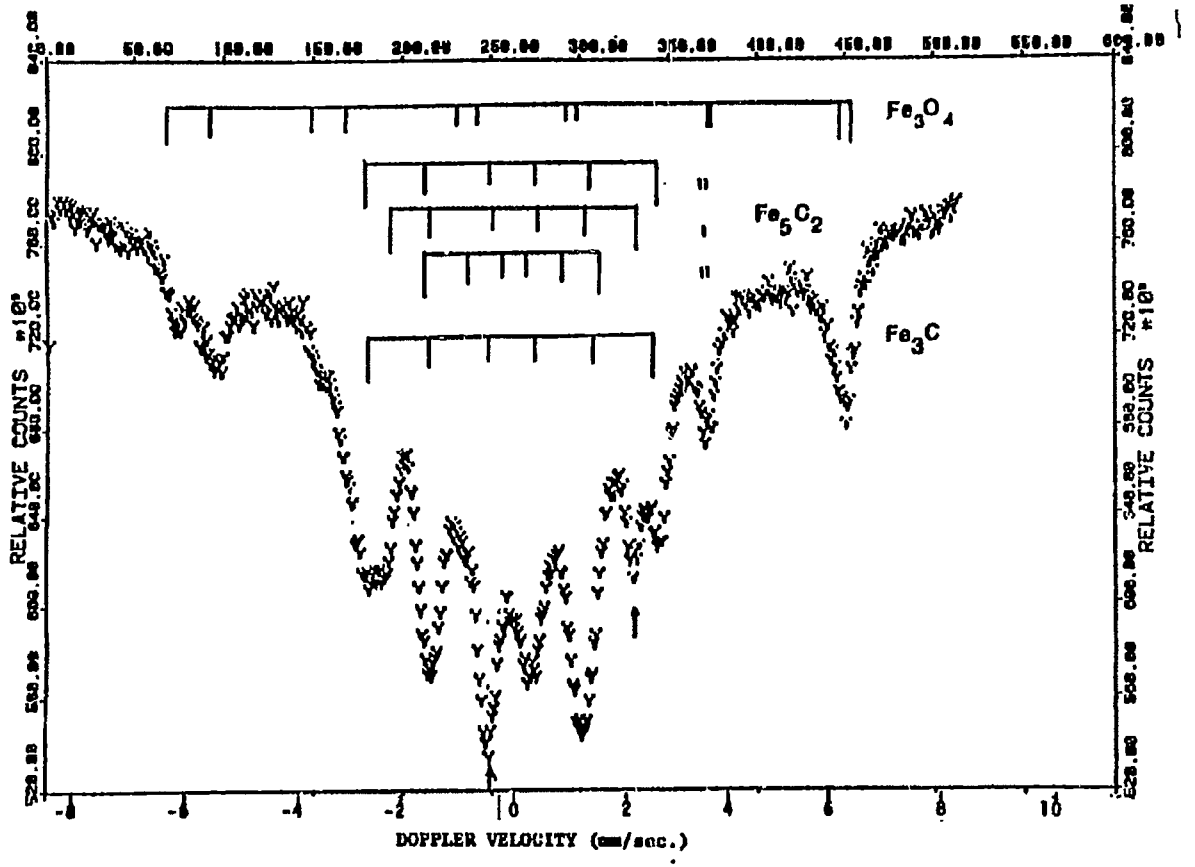

Figure 22. Mössbauer spectrum of used ZSM-5 (14.7% Fe)

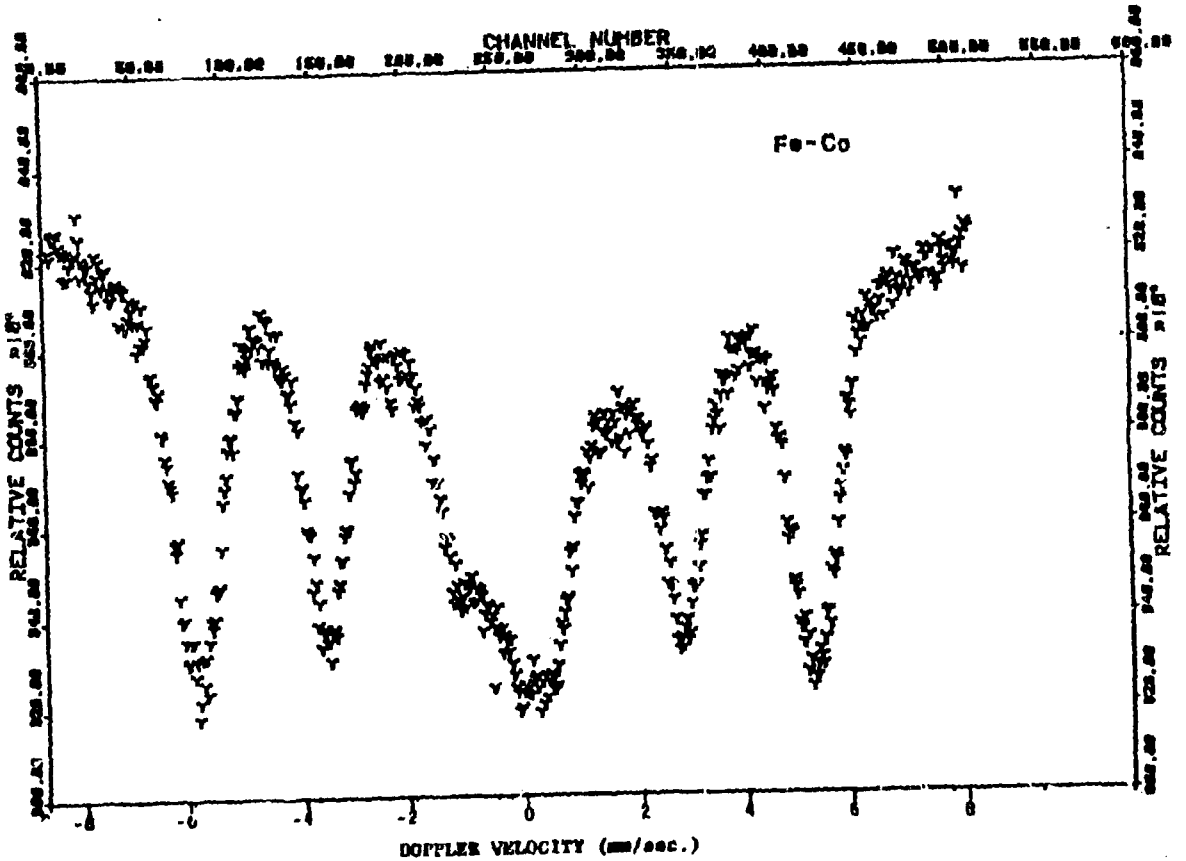

Figure 23. Mössbauer spectrum of use ZSM-5 (5.4% Fe, 4.5% Co)

The spectrum of used Silicalite containing 13.6% Fe is shown in Figure 24. It consists of both Hagg Carbide and Cementite and is similar to that observed for ZSM-5 with 14.7% Fe, except that this spectrum does not indicate the presence of any oxide. The spectrum of used Silicalite containing both 4.4% Fe and 3% Co is shown in Figure 25. This spectrum also contains Hagg Carbide and Cementite besides a strong doublet. However, the relative amounts of Hagg Carbide and Cementite present in this catalyst appear to be considerably less as compared with those in the catalyst containing only Fe. Thus, the presence of Co appears to hinder the formation of carbides in the Silicalite-based catalysts as well. Preliminary low temperature studies have shown that the central doublet is partly a result of superparamagnetic behavior of a magnetic phase.

The stick diagrams on various Mössbauer Spectra shown are the approximate line positions for Hagg (Fe_5C_2) and cementite (Fe_3C) phases and are drawn on the basis of Raupp and Delgass results (27).

The observation that the carbided ZSM-5 containing only Fe has relatively more Hagg Carbide compared to Cementite and that the used catalyst has, in contrast, relatively more Cementite than Hagg Carbide suggests that the Hagg Carbide has been converted into Cementite during the course of the reaction. Since synthesis gas conversion is exothermic, it is possible that local hot spots on the catalyst resulted in the conversion of the active Hagg Carbide to the relatively inactive Cementite phase. This could be partly the reason for the reduction in activity of these catalysts amounting to about thirty percent decrease over a period of two weeks exposure to synthesis gas at 280°C.

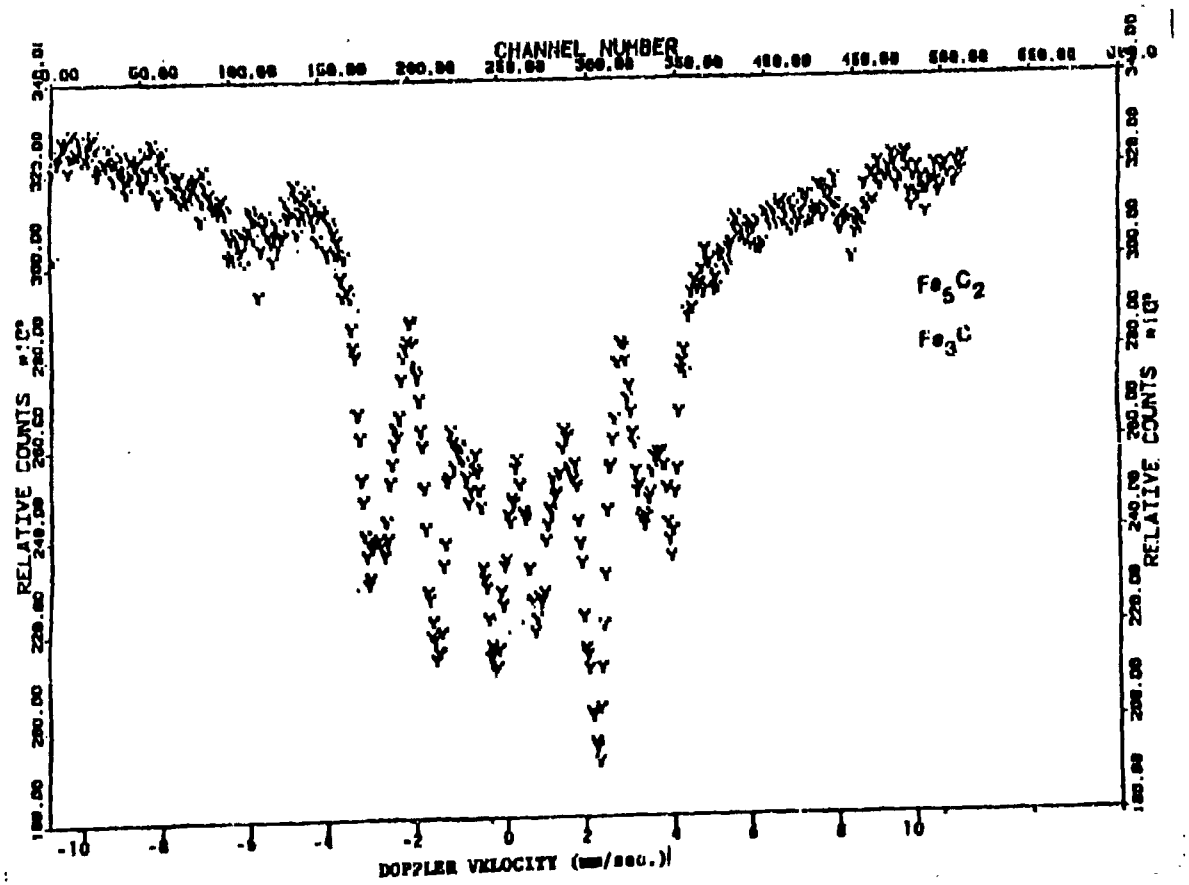

Figure 24. Mössbauer spectrum of used Silicalite (13.6% Fe)

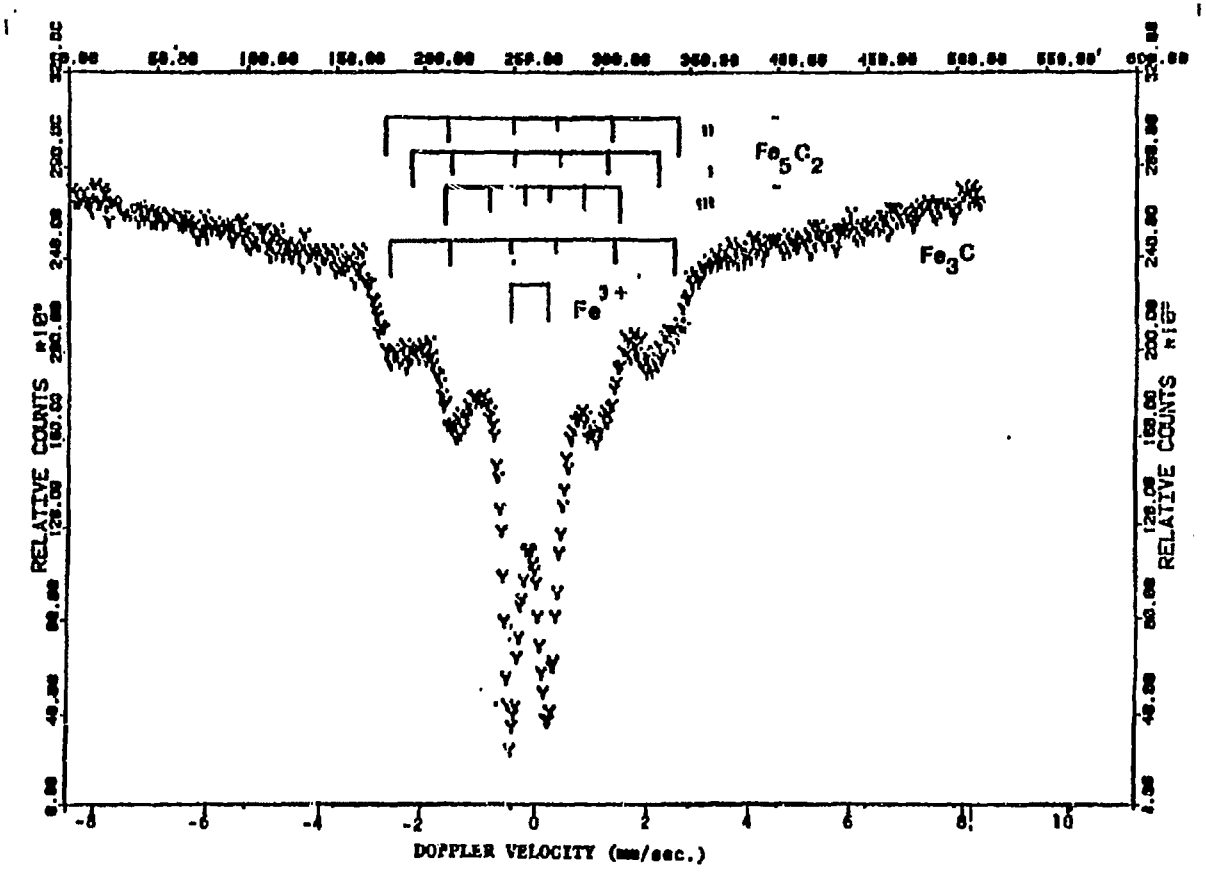

Figure 25. Mössbauer spectrum of used Silicalite (4.4% Fe, 3% Co)

B. Magnetic Measurements

The magnetization and susceptibility measurements were performed using the Faraday technique (65) in the temperature range 78 to 1000 K, and applied fields up to 20 KOe. A Cahn RH electrobalance was used for these measurements.

The freshly impregnated zeolites indicated the presence of Fe^{3+} species, from an analysis of the paramagnetic susceptibility, which showed an effective moment of ~5.96 Bohr Magnetons.

The magnetization studies on the reduced samples of ZSM-5 (14.7% Fe) and Silicalite (13.6% Fe) indicate that Fe is in the metallic state with 86% and 85% reduction, respectively. The magnetization versus temperature curves for ZSM-5 (11.1% Fe) are shown in Figure 26. The carbided sample of ZSM-5 (11.1% Fe) appears to be the high Curie point form (70) of the Hagg Carbide with T_C = 540K. The used sample of ZSM-5 (11.1% Fe) exhibited a magnetic transition with T_C = 650K which corresponds to the hcp phase of Fe_2C. The magnetic transition of Cementite (Fe_3C) was masked in the M vs. T curve shown in Figure 27 since T_C of Fe_3C is about 490K, well below that of the hcp carbide. The hcp phase of Fe_2C is considered to be stable (70) below 470K in an atmosphere of synthesis gas. Its presence in the used sample may indicate that it was formed while the catalyst was cooled after the reaction.

The magnetization data (Figure 27) on ZSM-5 (5.6% Fe, 4.5% Co) shows that the reduced, carbided and used samples have large magnetic moments (1,94, 2.04 and 2.61 μ_B per TM (transition-metal) atom respectively, at room temperature) and high Curie points (>900°C), which cannot be accounted for on the basis of individual Fe and Co

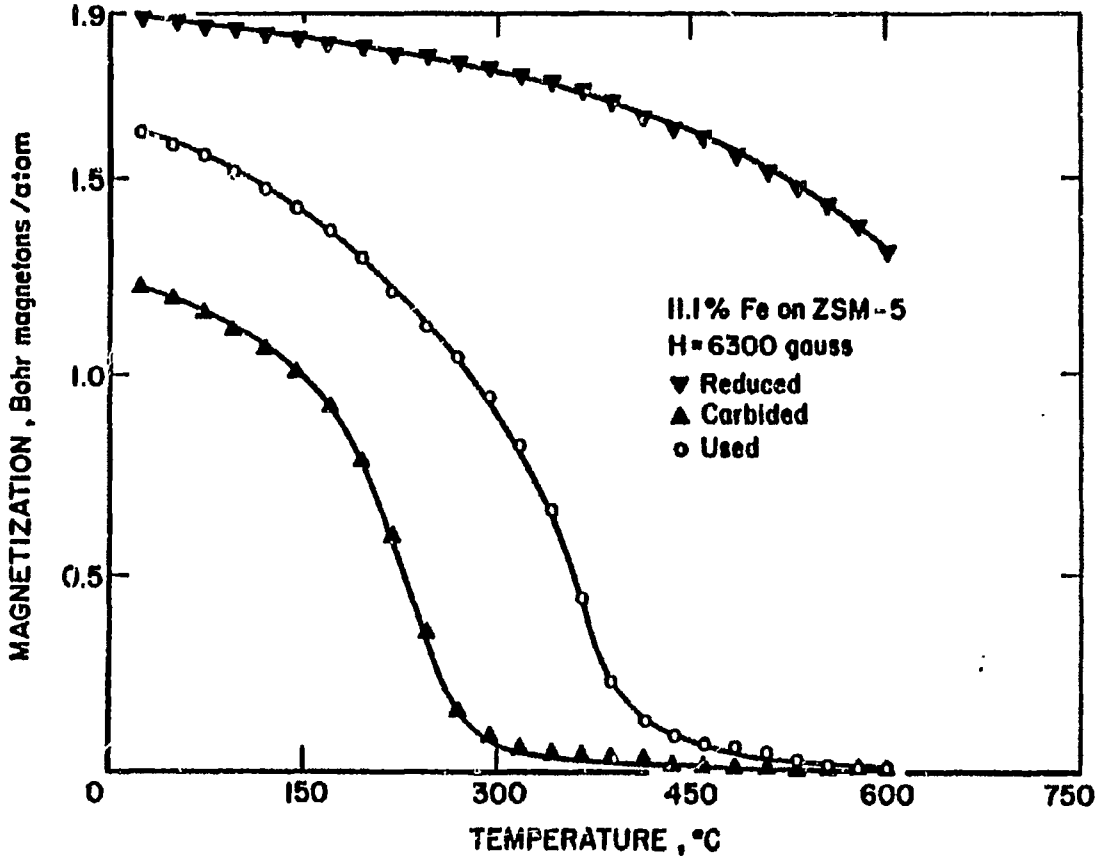

Figure 26. Magnetization (Bohr magnetons per Fe atom) as a function of temperature for ZSM-5 (11.1% Fe).

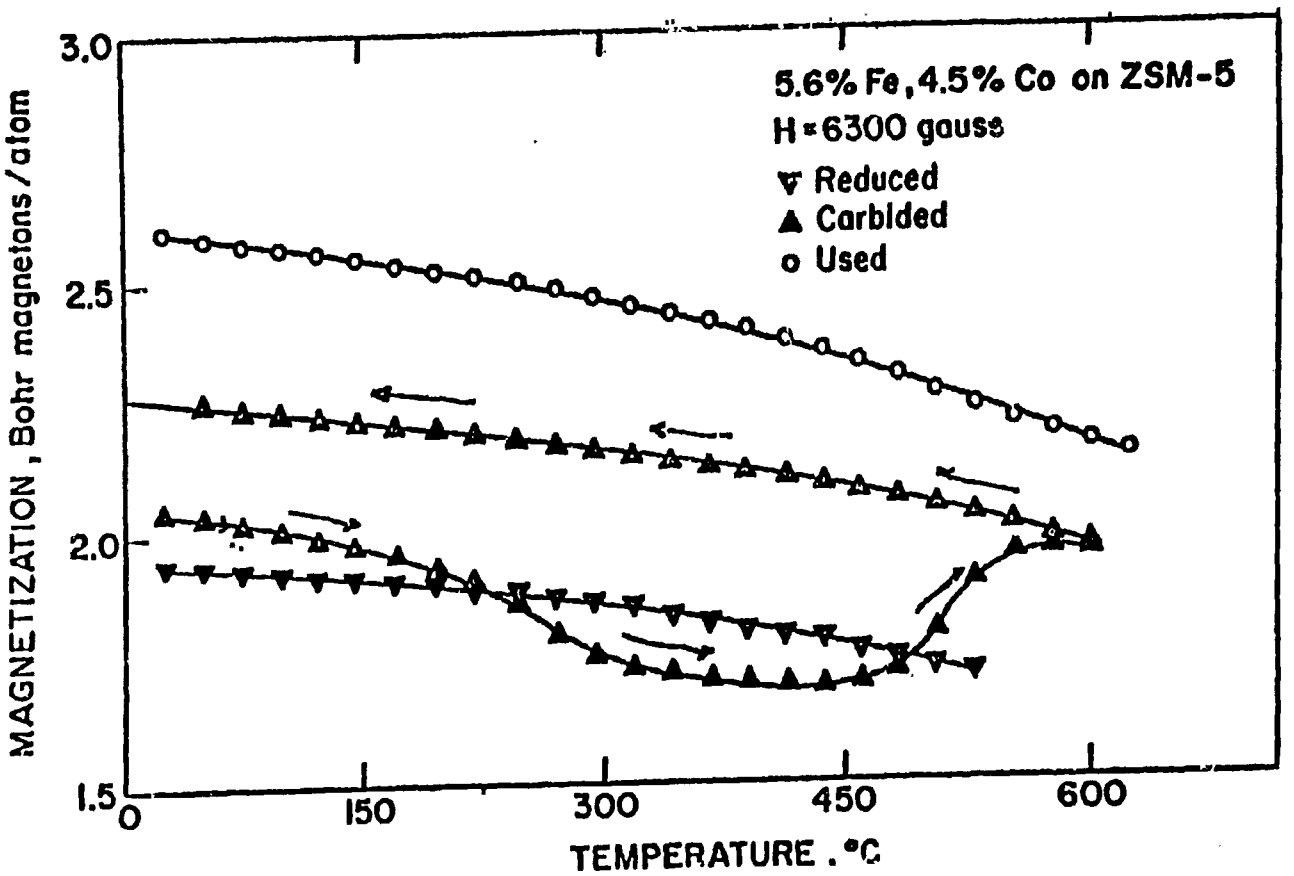

Figure 27. Magnetization as a function of temperature for ZSM-5 (5.6% Fe, 4.5% Co). The Bohr magneton number represents the weighted average of the two components present.

particles. The magnetic data indicate the composition to be that of a Fe-Co alloy (71), in support of the conclusions arrived through the Mossbauer analysis. Hence, one can conclude that the difference in selectivity between ZSM-5 (11.1% Fe) and ZSM-5 (5.6% Fe, 4.5% Co) catalysts (see Table 4) arises from the presence of bimetallic TM clusters in the latter, with consequent changes in the average number of 3d-electrons per TM atom. The M vs. T curve (Figure 27) of the carbided sample of ZSM-5 (5.6% Fe, 4.5% Co) indicated an irreversible formation of a second phase with a higher moment above a temperature of 450°C. This phase has not yet been identified.

4. Conclusions

A comparison of the spectra of carbided and used fe-ZSM-5 with those containing both Fe and Co, and their relative yields of aromatics (see Table 4) in the conversion process, and an overall consideration of all spectra and magnetic measurements indicate that

(a) the plausible active phase taking part in the conversion of the synthesis gas by Fe containing ZSM-5 and Silicalite is the Hagg Carbide which is converted into Cementite during the catalytic reaction,

(b) the difference in selectivity between ZSM-5 (Fe) and ZSM-5 (Fe + Co) arises from alloy formation in the latter which changes the 3d-electron concentration, and

(c) the increase in Co concentration in ZSM-5 (Fe + Co) results in decreasing carbide formation. This suggests that the Fe-Co alloy phase may itself be the active species in Co-rich catalyst compositions.

TABLE 4. Product Compositions from the Catalysts ZSM-5 (11.1% Fe) and ZSM-5 (5.6% Fe, 4.5% Co), in a Berty Reactor, Showing the Influence of cobalt addition to the Catalyst. Process Condition: $H_2/CO = 2$, P = 21 Bar

Catalyst	ZSM-5 (11.1% Fe)	ZSM-5 (5.6% Fe, 4.5% Co)
Temperature	300	280
CO Conversion, %	68.2	37.8
H_2 Conversion, %	38.7	41.3
Space Velocity	1500	1400
Product Composition (%)		
CO_2	52.0	9.8
H_2O	19.4	51.8
CH_n + Oxygenates	28.6	38.4
Hydrocarbon and Oxygenate Composition (%)		
C_1-C_4 hydrocarbons	83.1	74.3
C_5+ and Oxygenates	16.9	25.7
Composition of C_5+ and Oxygenates (%)		
Aromatics	72	10
Olefins	3	46
Saturates	24	37
Oxygenates	1	7
% Gasoline range (BP<204°C)	75	94
Research octane No.	96	81

REFERENCES

1. Storch, H.H., Golumbic, H., and Anderson, R.B., The Fisher-Tropsch and Related Synthesis, Wiley, New York (1951).

2. Pichler, H., Adv. Catal. 4, 271 (1952).

3. Vannice, M.A., Catal. Rev.-Sci. Eng. 14, 153 (1976).

4. Thomas, J.M. and Thomas, W.J., Introduction to Principles of Heterogeneous Catalysis, Academic Press, London (1967).

5. Carberry, J.J., Chemical and Catalytic Reaction Engineering, McGraw-Hill, New York (1976).

6. Cusumano, J.A., Dalla Betta, R.A., and Levy, R.B., Catalysis in Coal Conversion, Academic Press, New York (1978).

7. Shah, Y.T. and Perrotta, A.J., Ind. Eng. Chem. Prod. Res. Dev. 15(2), 123 (1976).

8. Biloen, P. and Sachtler, W.M.H., Mechanisms of Hydrocarbon Synthesis Over Fisher-Tropsch Catalysts, in Advances in Catalysis, Academic Press, New York (1971). (To be published.)

9. Mössbauer, R.L., Z. Phys. 151, 124 (1958).

10. Goldanskii, V.I. and Herber, P., Chemical Applications of Mössbauer Spectroscopy, Academic Press, New York (1968).

11. Greenwood, N.N. and Gibb, T.C., Mössbauer Spectroscopy, Chapman and Hall Ltd., London (1971).

12. Wertheim, G.K., Mössbauer Effect, Academic Press, New York (1971).

13. Bhide, R.L., Mössbauer Effect, Tata McGraw-Hill, New Delhi (1973).

14. Bancroft, G.M., Mössbauer Spectroscopy, Halsted Press, New York (1973).

15. Gütlich, P., Link, R., and Trautwein, A., Mössbauer Spectroscopy and Transition Metal Chemistry, Springer-Verlag Berlin Heidelberg, Germany (1978).

16. Delgass, W.N., Haller, G.L., Kellerman, R., and Lunsford, J.H., Spectroscopy in Heterogeneous Catalysis, Chap. 5, Academic Press, New York (1979).

17. Dumesic, J.A. and Topsøe, H., Adv. Catal. 26, 121 (1976).

18. Gager, H.M. and Hobson, Jr., Catal. Rev.-Sci. Eng. 11, 117 (1975).

19. Stevens, J.G. and Bowen, L.H., Anal. Chem. 50(5), 176R (1978).

20. Stevens, J.G. and Bowen, L.H., Anal. Chem. 52(5), 175R (1980).

21. Boudart, M., Delbouille, A., Dumesic, J.A., Khammouma, S., and Topsøe, H., J. Catal. 37, 486 (1975).

22. Dumesic, J.A., Topsøe, H., Khammouma, S., and Boudart, M., J. Catal. 37, 503 (1975).

23. Dumesic, J.A., Topsøe, H., and Boudart, M., J. Catal. 37, 513 (1975).

24. Dutartre, R., Bussière, P., Dalmon, J.A., and Martin, G.A., J. Catal. 59, 382 (1979).

25. Delgass, W.N., Garten, R.L., and Boudart, M., J. Chem. Phys. 50, 4603 (1969).

26. Raupp, G.B. and Delgass, W.N., J. Catal. 58, 337 (1979).

27. Raupp, G.B. and Delgass, W.N., J. Catal. 58, 348 (1979).

28. Raupp, G.B. and Delgass, W.N., J. Catal. 58, 361 (1979).

29. Maksimov, Y.V., Suzdalev, I.P., Arents, R.A., Goncharov, I.V., Kravtsov, A.V., and Loktev, S.M., Kinet. Catal. 13, 1425 (1973).

30. Maksimov, Y.V., Suzdalev, I.P., Arents, R.A., and Loktev, S.M., Kinet. Catal. 15, 1144 (1975).

31. Amelse, J.A., Butt, J.B., and Schwartz, L.H., J. Phys. Chem. 82, 558 (1978).

32. Huang, Y.Y. and Anderson, J.R., J. Catal. 40, 143 (1975).

33. Niemantsverdriet, J.W., van der Kraan, A.M., van Dijk, W.L., and van der Baan, H.S., J. Phys. Chem. 84, 3363 (1980).

34. Longworth, G. and Window, B., J. Phys. D. 4, 835 (1971).

35. Margulies, S. and Ehrman, J.R., Nucl. Inst. Methods, 12, 131 (1961).

36. Margulies, S., Debrunner, P. and Frauenfelder, H., Nucl. Inst. Methods, 21, 217 (1963).

37. O'Connor, D.A., Nucl. Inst. Methods, 21, 318 (1963).

38. Housley, R.M., Erickson, N.E. and Dash, J.G., Nucl. Inst. Methods, 29, 29 (1964).

39. Heberle, J., Nucl. Inst. Methods, 58, 90 (1968).

40. Mulay, L.N., in Physical Methods of Chemistry, Vol. 1, Part IIID, Edited by Weiseberger, A. and Rossiter, B.W., Wiley-Interscience, New York, 431 (1972).

41. Mulay, L.M. and Boudreaux, E.A., Theory and Applications of Molecular Diamagnetism, Wiley-Interscience (1977).

42. Mulay, L.N. and Boudreaux, E.A., Theory and Applications of Molecular Paramagnetism, Wiley-Interscience (1977).

43. Smart, J.S., Effective Field Theories of Magnetism, Saunders, Philadelphia (1966).

44. Chikazumi, S. and Charap, S.H., Physics of Magnetism, John Wiley and Sons, Inc., New York (1964).

45. Morrish, A.H., The Physical Principle of Magnetism, John Wiley and Sons, Inc., New York (1965).

46. Martin, D.H., Magnetism in Solids, Iliffe Books, Ltd., London (1967).

47. Turov, E.A., Physical Properties of Magnetically Ordered Crystals, Academic Press, New York (1965).

48. Van Vleck, J.H., Theory of Electric and Magnetic Susceptibilities, Clarendon Press, Oxford (1932).

49. Smart, J.S., in Vol. III of Magnetism, edited by Rado, G. and Subl, H., Chap. 2, Academic Press, New York (1963).

50. Selwood, P.W., Chemisorption and Magnetization, Academic Press, New York (1975).

51. Jacobs, I.S. and Bean, C.P., Magnetism, Vol. 3, Academic Press, New York (1963).

52. Cullity, B.D., Introduction to Magnetic Materials, Addison-Wesley, London (1972).

53. Michel, A., Ann. Chim. (Paris) 8, 317 (1937).

54. Michel, A., Bernier, R., and Le Clerc, G., J. Chim. Phys. 47, 269 (1950).

55. Frenkel, J. and Dorfman, J., Nature (London) 126, 274 (1930).

56. Elmore, W.C., Phys. Rev. 54, 1092 (1938).

57. Bean, C.P. and Livingston, J.D., J. Appl. Phys. 30, 1205 (1959).

58 Everson, R.C., Mahajan, O.P., Walker, P.L., Jr., and Mulay, L.N., J. Chem. Tech. Biotech. 29, 1 (1979).

59. Collins, D.W., Dehn, J.T. and Mulay, L.N., in Mössbauer Methodology, Vol. III, Gruverman, I.J., Ed. Plenum Press, N.Y. (1967).

60. Argauer, R.J., and Landolt, G.R., U.S. Patent 3,702,886 (1972).

61. Grose, R.W., and Flanigen, E.M., U.S. Patent 4,061,724 (1977).

62. Kokotailo, G.T., Lawton, S.L., Olson, D.H., and Meier, W.M., Nature 272, 437 (1978).

63. Flanigen, E.M., Bennett, J.M., Grose, R.W., Cohen, J.P., Patton, R.L., Kirchner, R.M., and Smith, J.V., Nature 271, 512 (1978).

64. Ruby, S.L., Mossbauer Effect Methodology, 8, 263 (1973).

65. Mulay, L.N., "Magnetic Susceptibility" (A reprint Monograph) Wiley-Interscience, New York (1966) (Available from Krieger Publications, New York, NY.). See also ref. 40.

66. Chang, C.D., Lang, W.H., and Silvestri, A.J., J. Catal. 56, 268 (1979).

67. Caesar, P.D., Brennan, J.A., Garwood, W.E., and Circ, J., J. Catal. 56, 274 (1979).

68. Rao, V.U.S., Gormley, R.J., Schneider, L.C., and Obermyer, R., Preprints, Div. of Fuel Chemistry, ACS, 25, 119 (1980).

69. Van der Woude, F. and Sawatsky, G.A., Physics Letters 12C, 335 (1974).

70. Sancier, K.M., Isakson, W.E., and Wise, H., Preprints, Div. of Petroleum Chemistry, ACS, 23(2), 545 (1978).

71. Bozorth, R.M., "Ferromagnetism," Van Nostrand, New York, pp. 190-209 (1951).

Appendix I

Contract No. DE-AC-22-79PC1035

Mössbauer Spectroscopic and Related Characterization of Fischer-Tropsch Catalysts

submitted by

Professor L. N. Mulay
Materials Research Laboratory
The Pennsylvania State University
University Park, PA 16802

to

U.S. Department of Energy
Pittsburgh Energy Technology Center
4800 Forbes Avenue
Pittsburgh, PA 15213

I. Introduction

As outlined in our ammended proposal of March 1, 1980, the work was undertaken to characterize a number "ZSM-5 and Silicalite - Fe, Fe-Co catalysts" mostly by Fe^{57} Mössbauer spectroscopy and related techniques such as magnetic measurements. As outlined in our detailed March 1980 annual report, attention was focussed on selected ZSM-5 and silicalite catalysts containing Fe or Fe-Co supplied by the Pittsburgh Energy Technology Center (PETC). This six-monthly report is an exploratory account of the work carried out since March 1980. This report should be regarded as factual in the sense that important Mössbauer spectra are presented without any final interpretations of the rather complex spectra observed with certain catalysts. The complexity arises, as one would expect. from the presence of more than one species, such as two or more iron-carbides, [each with ∿3 sites for Fe] and/or iron oxides. Our final interpretations must await computer fitting of the observed spectra to the known spectra reported for "pure" single phases.

II. Personnel

Dr. K.R.P.M. Rao, after obtaining a leave of absence from the Bhabha Atomic Research Center joined the project on October 15, 1979. He was paid from the project funds for about seven months (up to ∿May 15, 1980, when he was switched on to another project by the principal investigator, since sufficient funds were not available for his salary. (Only $4,952 from the first year + $7,980; a total of $12,932 were available.) Mr. Cary Lo (a Physics student) and Mr. Mehdi O'Tabrizi (a Solid State Science student) were each paid a half-time graduate assistantship for one term only; i.e. during the summer term-1980). Mr. Lo has replaced Dr. K.R.P.M. Rao and has assumed complete responsibility of the project.

III. New Instrumentation

A Mössbauer spectrometer for studies on the Fischer-Tropsch catalysts was set up and modified for low-temperature and/or applied external field work (4). We are currently using a new 25 mCi (milli Curie) source coupled to an "old" 15 mCi source. Thus we are using a relatively strong source (99 mCi) which is useful in quickly acquiring data on the F-T catalysts. The new source is Rh foil was supplied by the Spire Company, Bedford, MA.

A block diagram of the Mössbauer spectrometer and its associated electronics is shown in Figure A. The original Mössbauer drive unit and transducer for vibrating the source in the constant acceleration mode were manufactured by the Nuclear Science and Engineering Company, Pittsburgh, PA. This drive unit is now replaced by a brand new Austin Associates Drive unit with an absolute Neon-Laser velocity calibration. The gas proportional counter used to detect the 14.4 Kev gamma rays contained 90% krypton and 10% methane, and was made by the Reuter-Stokes Company, Cleveland, Ohio. The memory storage unit consists of a new ND-100 multichannel analyzer with 1026 channels, a single channel analyzer, high voltage supply, analog to digital converter, and a teletype and plotter drive, all of which are manufactured by the Nuclear Data, Inc., Chicago, IL. The teletype terminal was manufactured by the Teletype Corporation.

The new Austin Associates spectrometer provides (i) a sawtooth (ii) triangular and (iii) a sinnsoidal mode with capabilities for "constant velocity" operation, etc.

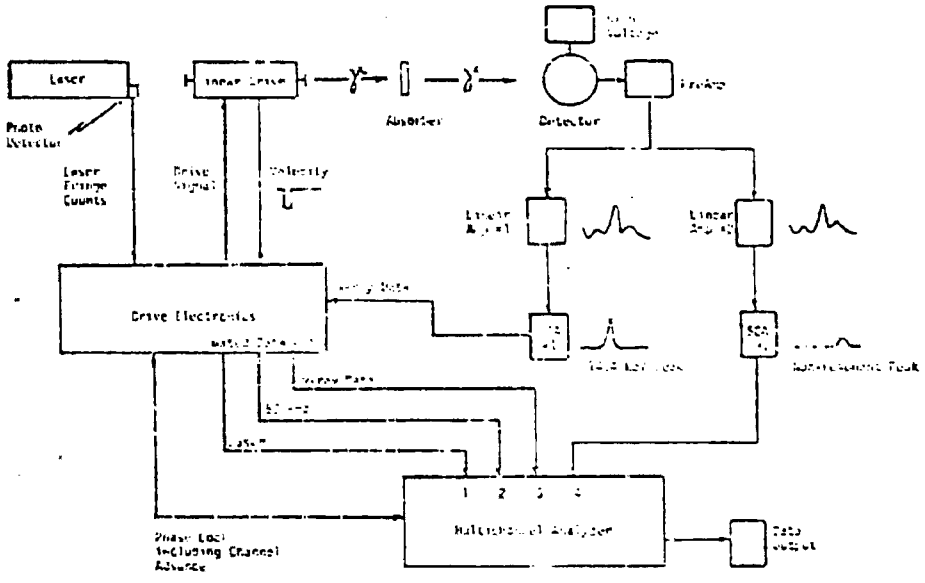

Fig. A Schematic of Mössbauer spectrometer configuration (with Laser).

IV. Methods of Measurement of Mössbauer Parameters

Samples for Mössbauer measurements were first ground to about 200 mesh in a dry-box when necessary. They were then weighed so that the thickness of the absorber consisted of about 30 mg/cm^2 of sample in order to prevent line broadening due to a thick absorber. Samples were spread onto an aluminum foil, 0.005" thick and of 99.999% purity, purchased from Alfa Products, Danvers, Massachusetts. The area of the sample was about 4 cm^2, so that 120 mg of sample was used for Mössbauer measurements. Collodion-acetone mixture was used to make the sample adhere to the aluminum foil.

The velocity of the drive unit was set so that all peaks of the spectrum were well contained within the 512 channels (or 1024) of the analyzer. Calibration was performed using an iron foil for which the six line positions occur at +5.0892, +2.8670, 0.6448, -1.0217, -3.2439 and -5.4662 mm/sec relative to Co^{57} in rhodium. The six lines of the iron spectrum also allow for a check of the linearity of the drive unit, which was found to be within ±0.5%. Since the channels for the peaks of the iron standard could be found from the printout sheet, a calibration constant in mm/sec/channel was calculated so that any channel number could be converted to a velocity.

Mössbauer spectra in an externally applied magnetic field were obtained in a few cases, and will be obtained in the future by using an electromagnet Model 1022 manufactured by Spectromagnetic Industries, Hayward, California with 16 cm diameter poles and an adjustable pole gap. The power was supplied by a current regulated power source, Model 6003, with a maximum current output of 110 amps. Tapered poles were used which had a minumum diameter of 3.5 cm. A pole gap of about 3 cm was used, which allowed a maximum field of about 20 KOe to be obtained in the gap. All measurements were made with the applied magnetic field perpendicular to the γ-ray beam.

All Mössbauer measurements below room temperature were performed using a Model LT-3-110 liquid transfer "Heli-Tran." The "Heli-Tran" was used in conjunction with an APD-E digital temperature controller, both of which were made by Air Products and Chemicals, Inc., Allentown, Pa. The aluminum foil containing the sample measurement was attached to a special sample holder supplied by Air Products and Chemicals, Inc., which was then screwed into the tip of the cold finger. The sample temperature could be maintained to ±0.10 K with this cyrostat. The thermocouple was calibrated by Air Products and Chemicals, Inc. For a detailed description of the theory and method of operation of the cyrostat, the reader should consult several excellent manuals written by Air Products and Chemicals, Inc.

V. Analysis of Mössbauer Data

The Mössbauer data was obtained from the spectrometer in the form of a paper tape and also printed on the teletype and recorded on the plotter. A computer program has been used in several cases and will be used extensively in the future to convert the contents of the paper tape onto a Cal-comp graphic converter. A least squares computer program obtained from the Quantum Chemistry Program Exchange and other groups in Bombay was used to fit the Mössbauer data. Single Lorentzians were used in fitting the spectra. The program was capable of varying the line positions, line widths and intensities in order to obtain the best fit. A fit was considered to be good when the chi squared value was approximately equal to the number of channels in the spectrum. In some cases, after an initial fit was obtained, the line widths were constrained and the fitting procedure was repeated. The line widths were usually constrained to be within 0.30 to 0.35 mm/sec, which is appropriate for Fe^{57}. For further details pertaining to the computer program used to fit Mössbauer data, the reader should consult Write Up No. 276 of Quantum Chemistry Program Exchange, Indiana University.

Several numerical methods have been developed for determining the hyperfine parameters from an observed Mössbauer spectrum: these being, in general, synthetic methods requiring a computer. As Hoy and Chandra (Cf 6) have pointed out, these approaches are unsatisfactory because they necessitate making successive fits to the observed spectrum, using trial and error values of the parameters. In view of these arguments, an analytical technique was adopted, which is discussed by Williams and Bancroft (Cf 6).

VI. Selected Magnetic Measurements

In an effort to supplement the Mössbauer results, we have carried out magnetization (σ, emu/g) measurements as a function of the field (H) at constant temperature(s) [T] with a vibrating sample magnetometer; thus the per gram susceptibility $\chi_g = \sigma/H$ could be obtained. In addition, we have occasionally used the more sensitive Faraday magnetic balance (1) in appropriate situations to measure the paramagnetic susceptibilities directly. It should be noted that for paramagnetics the molar susceptibility, χ_m, is a "good" parameter, whereas the magnetization (σ, emu/g) when measured as a function of (H/T) proves to be a better parameter for interpretations of a superparamagnetic system (2) which may or may not coexist with ferro- or ferrimagnetic components (3). The overall instrumentation was successfully completed during March-April-May 1979 as indicated in our original "Milestone" schedule. Mössbauer (and magnetic) characterization on all the samples (M-1 to M-9) was completed as planned.

VII. Synopsis of the Work Carried Out on the M-Samples sent by PETC During the Past Six Months:

The Mössbauer study of a number of bifunctional catalysts containing ZSM-5, silicalite or zeolite Nu-1 as the shape selective component, and Fe and/or Fe and Co as a transition metal component have been systematically studied. The catalysts were studied at various stages of preparation viz: when freshly prepared, reduced, carbides and finally after they were used in the Fischer-Tropsch conversion. The general findings of our study are outlined below:

(1) In the freshly prepared catalysts Fe^{3+} ions were found to exist, as expected.

(2) All the catalysts on reduction were found to contain either Fe metal when the catalyst had only Fe to start with, or a "Fe-Co alloy" when the catalyst was impregnated with "Fe and Co."

(3) On carburization of the ZSM-5 (Fe) samples at 250°C with 1:1 synthesis gas samples showed the presence of χ-carbides (Fe_5C_2) and cementite, (Fe_3C). It was found that the χ-carbide is dominant compared with the cementite phase.

A very interesting and significant result indicated that the addition of Co to the ZSM-5 (Fe) catalyst inhibited the formation of carbides in general. In particular, as increasing concentration of Co concentration, the formation of cementite decreased or almost inhibited.

(4) A conversion Electron Mössbauer Spectroscopy (CEMS or "Backscatter") study showed that as the Co concentration increases, the Fe carbides were not present on the top surface of the catalyst, at least in the upper 3000 Å thick surface. It is probable that cobalt is enriched on the surface of the catalyst. Independent ISS studies at PETC have also shown Co enrichment on the surface of ZSM-5 (Fe-Co) catalysts. This can explain changes in selectivity of the catalyst, such as reduction in CO_2 formation on the addition of even a small

amount of Co to a ZSM-5 (Fe) catalyst. This is a very important and a significant finding in the present study.

(5) The used catalysts showed the presence of carbides, with relatively more cementite as compared to the χ-carbide in contrast to the relative amounts of the two phases in the carbided samples. This indicates that the χ-carbide is converted to the cementite phase during the catalytic process of synthesis gas conversion. So it appears that the catalytically active phase is the χ-carbide while cementite (θ-Fe_3C) is less active.

In the following sections, we describe the specific details of the Mössbauer spectra observed for samples M-21 to M-25.

(6a) Sample M 21,

The Mössbuaer Spectrum of the fresh ZSM-5 with 10% Fe impregnated as $Fe_3(Co)_{12}$, consisted of a quadrupole doublet with a splitting of 0.81 mm/sec. and an isomer shift of 0.36 mm/sec. with respect to the α-Fe metal. The derived parameters indicated that the valence of Fe is in the catalyst is 3+.

(6b) Sample M 22,

The Mössbauer spectrum of a fresh sample of zeolite Nu-1 (10% Fe), impregnated using the carbonyl $Fe_3(CO)_{12}$ consisted of a broad and a rather poorly resolved doublet with a splitting approximately equal to that observed for M-21. It is possible that Fe ions in this catalysts are also in a 3+ valency state. There appears to be a superposition of a paramagnetic singlet on the quadrupole doublet; however, its origin is not understood at the present.

(6c) Sample 23,

The spectrum of the reduced ZSM-5 catalyst containing 10% Fe impregnates as $Fe_3(CO)_{12}$ consisted of a central broad line and a hyperfine spectrum corresponding to the Fe_3O_4 phase. So it appears that this catalyst could not be reduced to metallic iron as in other catalysts; it was converted to the magnetite phase, (Fe_3O_4) on reduction. The reason for this conversion to

an oxide on reduction is being probed.

Sample 24,

The Mössbauer spectrum of the reduced ZSM-5 containing 9% Fe and 9% Co consisted of a well resolved six finger pattern corresponding to an internal magnetic field (HFS) of 339 K Oe and an isomer shift of nearly zero with respect to α-Fe metal, which clearly indicated that this catalyst on reduction was converted into a "Fe-Co alloy." There is a very small unreduced Fe^{3+} component at the middle of the spectrum.

Sample 25,

The Mössbauer spectrum of the carbided catalyst ZSM-5 containing 9% Fe and 9% Co consisted of a complicated spectrum of a number of lines. It could be computer fitted to a set of 4 hyperfine fields corresponding to a Fe-Co alloy phase, (H = 340 KOe), and to the three inequivalent magnetic sites in a χ-carbide, (H_1 = 210 KOe, H_2 = 174 KOe and H_3 = 105 KOe). This it appears that the catalyst consists of an Fe-Co alloy and a χ-carbide phase. It is interesting to note that this catalyst did not contain any cementite phase (Fe_3C) unlike other ZSM-5 catalysts containing only Fe. This behavior suggests that the presence of Co in the catalyst has inhibited the formation of the cementite phase during carburization.

(7) Conversion Electron Mossbauer Spectroscopy (Backscatter) Study: (CEMS)

The CEMS spectrum of the carburized ZSM-5 containing 9% Fe and 9% Co surprisingly showed no Mössbauer lines indicating that there are no significant number of Fe atoms present in the top layer of about 3000 Å surface of the catalyst. As pointed out before, this seems to indicate that iron carbide formation on the top surface of the catalyst is prevented by the addition of Co to Fe. It is possible that the top layer of the catalyst may be just a carbon coating or may contain Co carbide(s). However, the CEMS of ZSM-5 containing only 14.7% Fe did give a Mössbauer spectrum of a complicated nature

but similar to that observed in the bulk sample of the catalyst by the conventional transmission Mössbauer spectroscopy.

The above two observations indicate that Co may be responsible for preventing the formation of a Fe-carbide phase at the surface of the catalyst.

The earlier ion scattering spectroscopy study of the catalyst, ZSM-5 containing 9% Fe and 9% Co at PETC, support our results in that the surface of the catalyst is seen to be rich in Co atoms.

(8) Plans for future work:

These have been outlined in detail in a one year renewal (ammended) proposal, (Mid September 1980). In general, we have been able to follow the milestone chart carefully. The principal investigator has made every effort to carry out research by (i) defining a problem - area in F-T catalysis (ii) by planning the experiments carefully (iii) by ex them thoroughly (iv) by booking all the information obtained from various techniques and (v) by doing a reasonable interpretation to seek "catalysts surface-properties" and "catalyst activity."

Appendix II

In-Situ Cell for Mossbauer Spectroscopy Study of Catalytic Reactions*

DESIGN AND CONSTRUCTION

Figure 1 is a side view of the cell with the sample holder block assembly in a raised position. A hollow boron nitride screw and stainless steel spacer hold a pressed sample wafer, 15.88 mm in diam, rigidly in a vertical position perpendicular to the gamma-ray transmission axis. In order to heat the wafer uniformly, four cartridge heaters (Hot Watt No. HS 252), connected in parallel, are placed in holes drilled into the cylindrical sample holder block from the top. The large mass of the stainless steel block helps to achieve a uniform and stable temperature. Temperature gradients in the region of the sample can be minimized by mounting ultrathin aluminum foil on the machined flat surfaces at the ends of the horizontal hole containing the absorber wafer. Two Chromel/Alumel thermocouples monitor temperature. One passes through a hole in the bottom of the sample holder block and touches the edge of the absorber wafer. The second touches the surface of the sample holder block in the annular space inside the cell. The thermocouple leads are connected through Chromel and Alumel solid-pin ceramic feedthroughs welded in the ConFlat flange. Reactant gases enter the cell through a 6.35 mm stainless steel tube welded to the sample holder block as shown in Fig. 1. Gases are preheated as they flow through the block. They then pass directly over the absorber wafer, giving maximum gas–sample contact. Gases exit through a 12.7 mm stainless steel tube to a vent. The exit line also serves as an evacuation port. Metal shutoff valves are Nupro SS-4BK-SW at the inlet, SS-4H-SW to the vent, and SS-8BK-SW to the vacuum system.

The sample holder block is welded to the upper part of the ConFlat flange through a stainless steel tube, machined to a wall thickness of 0.7 mm to reduce heat conduction. When the cell is evacuated, the annular space between the sample holder block and the outer shell of the cell provides good insulation. When the cell is run at atmospheric pressure, however, the outer shell heats up, and an additional heat shield is required to protect the Mössbauer source and the scintillation detector. The heat shield is a 180 mm long channel formed from 0.8 mm copper sheet with thin Be windows for gamma-ray transmission. The channel is set perpendicular to the gamma-ray transmission axis, and air is blown into it from both ends. With this arrangement, when the sample is at 773 K, the outer shell temperature is less than 523 K, and the source and detector remain at room temperature. In this configuration the minimum source to detector distance is 80 mm.

Since the outer shell can reach temperatures approaching 600 K, a key to the success of the device is a good seal between the Be window and the stainless steel. The windows, 22.9 mm in diameter and 0.254 mm thick, are specified to have 65 ppm Fe and were supplied by Kawecki Berylco Industries, Inc. To make the seal, ports were flanged out in the stainless steel 304 tube and seats machined as shown schematically in Fig. 2. The window was placed in the seat, and a Cu ring was placed at the Be–stainless steel step. A concentrating induction coil was used to melt the Cu in a vacuum of 1.33 $\times 10^{-4}$ Pa (10^{-6} Torr).

Fig 1 : See next page

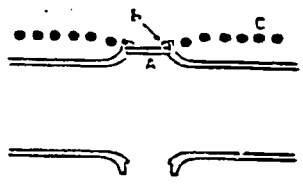

FIG. 2. Configuration of Be windows. A—window; B—copper ring; C—induction coil for vacuum brazing.

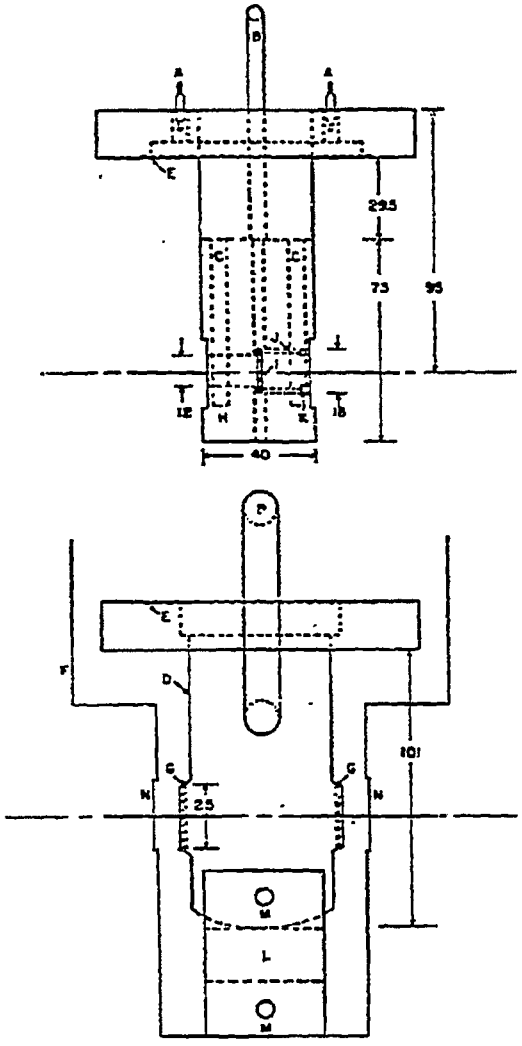

FIG. 1. Mössbauer absorber cell with the sample holder assembly raised and thermocouples, flange bolts, and bolt holes omitted. Dimensions in mm. A—Thermocouple feedthroughs; B—gas inlet tubing; C—heater wells; D—outer shell; E—gasket for ConFlat flange; F—copper heat shield; G—Be window; H—sample holder block; I—sample; J—retaining ring; K—hollow boron nitride screw; L—cell mount; M—screws to secure cell and mount; N—Be window; P—gas outlet.

*Based on paper by Delgass et al., Rev. Sci. Instrum. 47, 968 (1976).

U.S. DEPARTMENT OF COMMERCE
Technology Administration
National Technical Information Service
Springfield, VA 22161 (703) 605-6000